Atherosclerosis xxx (xxxx) xxx

Contents lists available at ScienceDirect

Atherosclerosis

journal homepage: www.elsevier.com/locate/atherosclerosis

Targeting LDL aggregation decreases atherosclerotic lipid burden in a humanized mouse model of familial hypercholesterolemia: Crucial role of ApoB100 conformational stabilization

A. Benitez-Amaro [a,b,1], E. Garcia [a,b,c,1], M.T. La Chica Lhoëst [a,b,c,1], A. Martínez [a,b], C. Borràs [d,e], M. Tondo [e,f], M.V. Céspedes [g,h], P. Caruana [g,h], A. Pepe [i], B. Bochicchio [i], A. Cenarro [j,k], F. Civeira [j,k], R. Prades [l], J.C. Escola-Gil [d,e], V. Llorente-Cortés [a,b,k,*]

[a] Institute of Biomedical Research of Barcelona (IIBB)-Spanish National Research Council (CSIC), 08036, Barcelona, Spain
[b] Institut d'Investigacions Biomèdiques IIB Sant Pau, 08041, Barcelona, Spain
[c] Universitat Autònoma de Barcelona, 08193, Bellaterra, Barcelona, Spain
[d] Institut de Recerca de l'Hospital Santa Creu i Sant Pau, Institut d'Investigacions Biomèdiques IIB Sant Pau, 08041, Barcelona, Spain
[e] CIBER de Diabetes y Enfermedades Metabólicas Asociadas (CIBERDEM), 28029, Madrid, Spain
[f] Department of Clinical Biochemistry, Hospital de la Santa Creu i Sant Pau, IIB Sant Pau, 08041, Barcelona, Spain
[g] Grup d'Oncologia Ginecològica i Peritoneal, Institut de Recerca Sant Pau, Hospital de la Santa Creu i Sant Pau, 08041, Barcelona, Spain
[h] Universitat de Barcelona (UB), 08007, Barcelona, Spain
[i] Laboratory of Bioinspired Materials, Department of Science, University of Basilicata, Potenza, Italy
[j] Hospital Universitario Miguel Servet, IIS Aragón, Instituto Aragonés de Ciencias de la Salud, Universidad de Zaragoza, Zaragoza, Spain
[k] CIBER de Enfermedades Cardiovasculares CIBERCV, Institute of Health Carlos III, 28029, Madrid, Spain
[l] Iproteos S.L., Barcelona Science Park (PCB), Barcelona, Spain

ARTICLE INFO

Keywords:
Atherosclerosis
LDL aggregation
LRP1-Based peptides
ApoB100 conformation
Therapeutic peptides

ABSTRACT

Background and aims: Low-density lipoprotein (LDL) aggregation is nowadays considered a therapeutic target in atherosclerosis. DP3, the retro-enantio version of the sequence Gly^{1127}-Cys^{1140} of LRP1, efficiently inhibits LDL aggregation and foam cell *in vitro* formation. Here, we investigate whether DP3 modulates atherosclerosis in a humanized ApoB100, LDL receptor (LDLR) knockout mice (*Ldlr*$^{-/-}$*hApoB*100 Tg) and determine the potential LDL-related underlying mechanisms.

Methods: Tg mice were fed an HFD for 21 days to induce atherosclerosis and then randomized into three groups that received a daily subcutaneous administration (10 mg/kg) of i) vehicle, ii) DP3 peptide, or iii) a non-active peptide (IP321). The *in vivo* biodistribution of a fluorescent-labeled peptide version (TAMRA-DP3), and its colocalization with ApoB100 in the arterial intima, was analyzed by imaging system (IVIS) and confocal microscopy. Heart aortic roots were used for atherosclerosis detection and quantification. LDL functionality was analyzed by biochemical, biophysical, molecular, and cellular studies.

Results: Intimal neutral lipid accumulation in the aortic root was reduced in the DP3-treated group as compared to control groups. ApoB100 in LDLs from the DP3 group exhibited an increased percentage of α-helix secondary structures and decreased immunoreactivity to anti-ApoB100 antibodies. LDL from DP3-treated mice were protected against passive and sphingomyelinase (SMase)-induced aggregation, although they still experienced SMase-induced sphingomyelin phospholysis. In patients with familial hypercholesterolemia (FH), DP3 efficiently inhibited both SMase-induced phospholysis and aggregation.

Conclusions: DP3 peptide administration inhibits atherosclerosis by preserving the α-helix secondary structures of ApoB100 in a humanized ApoB100 murine model that mimicks the hallmark of human hypercholesterolemia.

* Corresponding author. Institute of Biomedical Research of Barcelona (IIBB)-Spanish National Research Council (CSIC), 08036, Barcelona, Spain.
E-mail address: cllorente@santpau.cat (V. Llorente-Cortés).
[1] These authors equally contributed.

https://doi.org/10.1016/j.atherosclerosis.2024.118630
Received 21 February 2024; Received in revised form 30 September 2024; Accepted 15 October 2024
Available online 19 October 2024

1. Introduction

Atherosclerosis is a highly prevalent disease in persons with dyslipidemia, metabolic disorders, and obesity. Low-density lipoproteins (LDLs) are the main carriers of cholesterol in blood and are often entrapped in the network of proteoglycans that structure the extracellular matrix (ECM) of the arterial intima [1–3]. LDLs retained in the vascular wall become aggregated, mainly due to the actions of lipolytic enzymes present in the arterial intima. Phospholypolysis causes strong alterations in the original ApoB100 structural conformation, which mainly contribute to LDL aggregation susceptibility [4,5]. Aggregated LDL is an important source of cholesterol for the vasculature largely due to its uptake by low-density lipoprotein receptor–related protein 1 (LRP1), which, in contrast to LDLR, is not downregulated by intracellular cholesterol [6–8]. As LRP1 is upregulated by hypoxia, the receptor is highly efficient in generating intracellular lipid-droplet (LD) and prothrombotic cell phenotypes in the arterial intima [9–11]. Currently, both LDL susceptibility to aggregation [12–14] and increased presence of the soluble form of LRP1 (sLRP1) [15,16] are known to be associated with future adverse cardiovascular events in humans.

Our group identified for the first time a new epitope in ApoB100 that recognizes a particular LRP1 sequence named P3 (Gly^{1127}-Cys^{1140}) located in the CR9 domain of cluster II of LRP1 [17,18]. The capacity of DP3 to establish electrostatic interactions with ApoB100 facilitate the formation of DP3/ApoB100 complexes that efficiently keep ApoB100 structure, inhibiting LDL aggregation [18]. Not only that, the formation of this complex also prevents the interaction between ApoB100 and LRP1 inhibiting aggregated LDL uptake and foam cell formation [17–19]. Therefore, these peptides offer the unprecedent possibility to efficiently block smooth muscle cell foam cell formation acting at the extracellular level, modulating LDL atherogenicity, without altering LRP1 essential signaling, and thus with low potential off-target effects.

LDL propensity to aggregation depends on the LDL quality [12–14], which, in addition to LDL quantity and years of increased LDL levels [20], should be clinically considered to predict atherosclerotic plaque burden in humans. Currently, apolipoprotein-based peptides with the capacity to inhibit LDL aggregation have emerged as potential therapeutic tools for atherosclerosis (reviewed in Ref. [21]). These Apolipoprotein-based peptides are usually designed as short amino acid chains based on functional domains of ApoA-I [22] and ApoJ [23,24]. These peptides share an amphipathic nature that facilitates their efficacy to rearrange lipids, in particular phospholipids, thereby conferring stability to LDL.

Differently to ApoB-based peptides that interact with phospholipids, LRP1-based peptides designed by our group target the particular sequence of ApoB100 involved in protein aggregation. Of particular interest is the retro-enantio D-peptide version of P3, DP3 (H-needsn-desdndh-$CONH_2$), whereby the amino acid letter code in lowercase stands for amino acids with D-chirality; of note, DP3 maintains the acidic residues essential for the interaction with apolipoprotein (Apo) B100 (Glu^{1132}, Asp^{1133} and Glu^{1138}), and has higher permeability and stability than the original LP3 peptide [18,19]. DP3 has been shown to efficiently block LDL aggregation (by more than 90 %) and foam cell formation from human coronary vascular smooth muscle cells [17–19] and tumor pancreatic cells [25]. These previous findings prompted us to investigate the effects of one of the most promising peptides, DP3, in a translational ApoB100 humanized murine model.

Our main objective here was to investigate the effects of DP3 on HFD-induced atherosclerosis in a humanized ApoB100 murine model, and to determine the mechanisms underlying the potential *in vivo* DP3 effects.

2. Materials and methods

2.1. Animal studies

2.1.1. Generation of the animal model

All animal procedures were conducted in accordance with published regulations and reviewed and approved by the Institutional Animal Care Committee of the Research Institute of the Hospital de la Santa Creu i Sant Pau (reference number 10626). Wild-type mice and total $Ldlr^{-/-}$ mice on the C57BL/6J background were purchased from Jackson Laboratories (Bar Harbor, ME; #00064 and #002207, respectively) and C57BL/6J and human ApoB100 transgenic (*Ldlr*+/+ *hApoB*100 Tg) mice were purchased from Taconic Biosciencies (Rensselaer, NY; catalog #1004-M). $Ldlr^{-/-}$ mice were crossbred with *hApoB*100 Tg mice to generate heterozygous $Ldlr^{+/-}$ mice expressing hApoB100 (*Ldlr* ±*hApoB100*). *Ldlr* ±*hApoB100* were crossbred with $Ldlr^{-/-}$ to generate $Ldlr^{-/-}$ mice expressing hApoB100 ($Ldlr^{-/-}$hApoB100 Tg) (online Fig. S1). Mice were genotyped by PCR analysis using tail tip genomic DNA with primers for LDLr (common forward primer: 19799, wild-type reverse primer: 19800, and mutant reverse primer: olMR7770, TIB MolBiol), whereas hApoB100 transgenic mice were detected by testing the serum levels of hApoB100 with an immunoturbidimetric assay adapted for a COBAS 6000/501c autoanalyzer (Roche Diagnostics, Rotkreuz, Switzerland).

2.1.2. Experimental design for induction and treatment of atherosclerosis in vivo

Female mice were used in this experimental procedure due to the capacity of females to develop advanced atherosclerotic plaques earlier than males [26]. In addition, mice were fed a western-type diet (TD.88137, Harlan Teklad, Madison, WI, containing 21 % fat and 0.2 % cholesterol) to induce atherosclerotic lesions in less than one month (in 3 weeks). At this short time of diet, we only observed atherosclerotic lesions in the aortic root but not in the aorta. Therefore, the use of females and high-fat diet in this experimental model is justified because it implies a shortening of animal treatment to obtain a proof-of-concept of DP3 efficacy. Mice were kept in a temperature-controlled (22 ± 0.2 °C) room with a 12-h (h) light/dark cycle and provided food and water *ad libitum*. As shown in Fig. 3A, 8-to 12-week-old female mice were randomized to the intervention DP3-treated group, IP321-injected group or to a group without peptide injection as controls. During the intervention dietary period, mice received a daily subcutaneous injection with either DP3 (DP3 group, 10 mg/kg in cyclodextrin, 5 mL/kg) or IP321 (IP321 group, 10 mg/kg in cyclodextrin, 5 mL/kg). An additional control group was injected with cyclodextrin (vehicle). Blood samples were collected before (pre-diet) and 3 weeks after diet (post-diet) for biochemical and lipid profile analyses.

2.1.3. In vivo biodistribution of DP3 peptide

Female mice were fasted for 3 h prior to the biodistribution experiments to avoid the presence of intestinal food as a potential source of fluorescence. In addition, the abdomen of mice was shaved to obtain an optimal fluorescence signal.

Mice were intravenously injected with a fluorescent version of the peptide (TAMRA-DP3, 50 mg/kg in 10 % cyclodextrin, 7.14 mL/kg). Mice were injected at 60, 30 and 15 min before euthanasia (Fig. 2A). Fluorescence image (FLI) at emission and excitation of 500–540 nm, respectively, were measured using the Spectrum 200 *in vivo* Imaging System (IVIS, PerkinElmer). Prior to peptide injections, the fluorescence emitted by the peptide at the administration volume and dose was measured as the control of fluorescence charge. The autofluorescence of each mouse before the peptide injection was considered the basal fluorescence and subtracted from post-injection fluorescence values. After recording the whole-body mouse *in vivo* fluorescence, mice were euthanized and necropsied. The fluorescence of the different organs of interest was also measured *ex vivo* in the IVIS equipment immediately

after removal from the mouse.

2.1.4. Anesthesia and euthanasia

Isoflurane was used for sedation with a concentration of 4–5% in the induction phase and 1–2% for maintenance. The effect was monitored by the animal's loss of reflexes. For anesthesia before euthanasia, a mixture of medetomine and ketamine was administered subcutaneously in the proportion of 1:75 initially and subsequently at 1:100. The effect was monitored by controlling adequate muscle relaxation, without vocalizations and without movements in response to stimulation. Finally, euthanasia was carried out by cervical dislocation.

2.2. Characteristics of patients with hypercholesterolemia

This study includes 13 patients, aged 23–70 years, with the diagnosis of primary hypercholesterolemia recruited in the Lipid Unit of Hospital Universitario Miguel Servet. Primary hypercholesterolemia was diagnosed when the plasma off-treatment LDL cholesterol (LDL-C) concentrations exceeded the age and sex-specific 95th percentiles of a Spanish reference population [27]. Other inclusion criteria were a body mass index (BMI) < 30 kg/m^2, a steady weight (± 3 kg in the previous 3 months), plasma triglyerides (TG) < 300 mg/dL, and no intake of lipid-lowering drugs (including plant sterol/stanol supplements) in the previous 5 weeks. Exclusion criteria were alcohol consumption >30 g/day, uncontrolled type 2 diabetes (glycated hemoglobin >8 %), or any other chronic disease that could interfere with lipid metabolism. All patients provided written informed consent prior to enrollment.

Clinical variables registered during visits included diabetes, hypertension, smoking, weight, height, waist circumference, and blood pressure. Plasma samples were obtained after overnight fasting, and total cholesterol, triglycerides (TG), and high-density lipoprotein cholesterol (HDL-C) were measured by standard enzymocholorimetric methods. LDL-C was estimated by the Friedewald formula, while ApoB100, ApoA-I and C-reactive protein (CRP) were determined by nephelometry. Patient characteristics are summarized in online Table S1.

2.3. Peptide synthesis, labeling, and purification

Peptide sequences are given from N-terminal to C-terminal, whereby H– at the end terminus indicates an amine (H_2N-) ending, whereas –$CONH_2$ at the C-terminus indicates amide. The amino acid sequence of the LP3 peptide (parent) is H-GDNDSEDNSDEENC-$CONH_2$; DP3 is the retro-*enantio* version of LP3 without cysteine, of H-needsndesdndh-$CONH_2$, whereby the amino acid letter code in lowercase stands for amino acids with D-chirality. The negative control was an ApoB100-based peptide coded as IP321 with the sequence H-RLTRKRGLK-NH_2. All peptides were synthesized by Iproteos using 9-fluorenylmethoxycarbonyl/tert-butyl (Fmoc/*t*Bu) strategy in solid-phase. Syntheses were performed manually on a 100-μmol scale/each using Rink amide ChemMatrix® resin. Peptide elongation and other solid-phase manipulations were done manually in polypropylene syringes, each fitted with a polyethylene porous disk. Solvents and soluble reagents were removed by suction. Washings between synthetic steps were done with dimethylformamide and dichloromethane, using 5 mL of solvents/g resin each time. *Nα*-Fmoc-protected amino acids (4 equivalents) were coupled using 2-(1H-benzotriazole-1-yl)-1,1,3,3-tetramethyluronium (TBTU, 4 equivalents), and *N*, *N*-diisopropylethylamine (8 equivalents). The extent of the reaction was monitored using the Kaiser test. During couplings, the mixture was allowed to react with intermittent manual stirring. The Fmoc group was removed by treating the resin with 20 % piperidine in (N, N-dimetilformamide) DMF (3 mL/g resin). Peptides were cleaved from the resin using a mixture of trifluoroacetic acid, triisopropylsilane and water (95:2.5:2.5). The crude products obtained were purified in reverse phase using a semi-preparative HPLC instrument equipped with a C18 column. The purity and identity of the synthesized peptides was assessed by HPLC, HPLC-MS and MALDI-TOF analysis. TAMRA-DP3 was obtained from Schafer-N (Denmark) according to their internal peptide procedures.

2.4. Blood collection from FH patients

Blood collection and processing were conducted according to the Standard Operating Procedures for Serum and Plasma Collection established by the Early Detection Research Network Consensus Statement and Standard Operating Procedure Integration Working Group [28]. Venous whole blood samples were drawn into 10 mL Vacutainer EDTA tubes (BD) by venipuncture after a night of fasting. The tubes were immediately inverted 8–10 times. Blood was processed within 2 h of extraction. Plasma was separated by centrifugation at $1300\times g$ for 15 min at room temperature. After centrifugation, the plasma was carefully transferred to 1.5 mL DNA LoBind tubes, leaving approximately 1 mL of plasma above the buffy coat, and stored at −80 °C. LDL was then isolated from the plasma.

2.5. Blood collection and monocyte quantification in the in vivo model

Whole blood (150 μL) from mice was lysed using Red Blood Cell Lysis Solution from Miltenyi Biotec, following the manufacturer's instructions. Cells were centrifuged at $300\times g$ for 10 min, washed, and resuspended in PBS 1X. An aliquot of the cell suspension (93 μL) was stained with Viobility 405/520 Dye and incubated with antibodies CD11b-Vio Blue, F4/80-FITC, CD45-PE, CD3e/CD19/CD335-PerCPVio700, Ly6C-PEVIO770, and Ly6G-APC (all from Miltenyi Biotech) at a 1:50 dilution for 15 min at room temperature, according to the datasheet. Cells were washed once with PEB buffer (Miltenyi Biotec) and resuspended in PBS 1X. Cell analysis was performed using a MacsQuant 10 Flow Cytometer as detailed in online Fig. S2.

2.6. Culture of smooth muscle cells (SMC)

Cells from a single lot batch (61646600) obtained from ATCC (ATCC-PCS-100-021) were used to minimize variability from different cell sources. Quiescence was induced by maintaining the cell culture for 24 h in medium containing 0.2 % fetal calf serum or for 48 h in medium with 0.4 % serum at 37 °C and 5 % CO_2. Serum-deprived cells between passages 4 and 8 were used for experiments. Cells at these passages exhibited a relatively homogeneous population with a hill-and-valley confluence pattern. Cell monolayers were cultured in vascular cell basal medium (ATCC-PCS 100-030) supplemented with components from the vascular smooth muscle growth kit (ATCC-PCS-100-042). Quiescent cells were exposed to LDL, which had been treated with SMase for 18 h in the presence or absence of peptides at a concentration of 10×10^{-6} M, for 2 h. The degree of LDL aggregation was assessed by turbidimetry measurements before incubation with the cells. Cells were then collected for lipid extraction, followed by neutral intracellular lipid partitioning through thin-layer chromatography and lipid band analysis and quantification.

2.7. Biochemical studies

Plasma total and lipoprotein content of cholesterol and TG were determined enzymatically by using commercial kits adapted for a COBAS 6000/501c autoanalyzer (Roche Diagnostics, Rotkreuz, Switzerland). HDL-C levels were measured in serum obtained after the precipitation of ApoB-containing lipoprotein particles with 0.44 mmol/L phosphotungstic acid (Merck, Darmstadt, Germany) and 20 mmol/L magnesium chloride (Sigma-Aldrich, St Louis, MO). VLDL (1.006 g/mL), LDL (1.019–1.063 g/mL), and HDL (1.063–1.210 g/mL) lipoproteins were isolated from the serum via sequential ultracentrifugation, using potassium bromide (KBr) for density adjustment, at 36,000 *g* for 24 h with an analytical fixed-angle rotor (Beckman Coulter, Fullerton, CA). Serum and lipoprotein levels of hApoB100 were measured using an

immunoturbidimetric assay adapted for the COBAS 6000/501c auto-analyzer (Roche Diagnostics, Rotkreuz, Switzerland).

2.8. Polyacrylamide gradient gel electrophoresis

Polyacrylamide gradient gel electrophoresis was used to separate ApoB100 and ApoB48 in lipoprotein samples. Gradient gels were prepared with 5 % and 15 % acrylamide solutions, using a stock solution of 30 % acrylamide and 5 % bis-acrylamide (total 35 %). The gradient was created with two P-1 peristaltic pumps (Pharmacia). Samples (5 μL at 1.44 mg/mL) were preincubated for 15 min with 10 μL of Sudan Black (0.1 % [wt/vol]) in ethylene glycol and 5 μL of sucrose (50 % [wt/vol]). Ten microliters of the preincubated sample mixture were electrophoresed at 4 °C with a sequential voltage protocol: 30 min at 20 V, 30 min at 70 V, and 4 h at 100 V. Bands were then analyzed using densitometry.

2.9. Reverse transcription and real-time qPCR analysis

Total liver RNA was isolated using the Total RNA Extraction Kit (Sigma) and quantified with a NanoDrop ND-1000 spectrophotometer (NanoDrop Technologies). RNA was then reverse-transcribed using the RevertAid First Strand cDNA Synthesis Kit (Thermo Scientific). The 18S rRNA gene was used as a housekeeping gene. Quantitative real-time PCR (qRT-PCR) was performed using TaqMan assays for TNFα (Mm99999068_m1), CCL2 (Mm00441242_m1), CD36 (Mm00432403_m1), and CD68 (Mm03047343_m1) on the 7900HT Fast Real-Time PCR System (AB-Thermo Fisher Scientific).

2.10. Thin layer chromatography of neutral lipid content in smooth muscle cells (SMCs) and murine livers

The neutral lipid content of cholesteryl ester (CE), triglycerides (TG), and free cholesterol (FC) was determined by thin-layer chromatography (TLC) following lipid extraction of smooth muscle cells (SMCs) or hepatic tissue. Lipids were extracted using a dichloromethane/methanol [1:2] solvent mixture. CE, FC, and TG were separated on silica G-24 TLC plates as previously described [8–10]. Standards consisting of cholesterol, cholesterol palmitate, and triglycerides were applied to each plate. The spots corresponding to CE, TG, and FC were quantified by densitometry against standard curves for cholesterol palmitate, triglycerides, and cholesterol, respectively, using a computing densitometer. Results were expressed as the ratio of CE to FC in each LDL sample.

2.11. Bioimaging evaluation of atherosclerotic lipid burden

Mouse hearts (n = 7/group) were isolated, cryopreserved with saccharose 30 % overnight, fixed in 4 % formaldehyde, and divided in two parts. The upper portion containing the aortic root and aortic valve was separated, embedded in optimal cutting temperature (OCT) (VWR, Fontenay-sous-Bois, France), and immediately flash frozen for atherosclerotic plaque evaluation, as previously described [29,30]. Serial cross-sectioning (7 μm) of the aortic root was performed and the quantification of neutral lipid accumulation was analyzed at the beginning and in the middle of the aortic valve. The lipid component of the lesions (surface area stained with Oil Red O) was quantified using AxioVision V 4.8.1.0 image analysis software (Zeiss, Oberkochen, Germany) and shown as percentage of the total vessel area. The vascular colocalization of ApoB100 with DP3 in the atherosclerotic lesions was evaluated in specific aortic root sections previously characterized according to Oil Red O. Tissue sectioning of kidney was performed to detect the levels of excreted DP3 peptide. Peptide levels in aortic root and kidney, and colocalization of peptide with human ApoB100 in aortic root were observed by Zeiss LSM780 confocal microscope.

2.12. Studies about the susceptibility of LDL to aggregation

2.12.1. Lipoprotein isolation and purification

Plasma samples from every three animals were combined to generate pooled samples sets (six pools per group, n = 18/group) to ensure sufficient volume for isolating quantifiable levels of lipoproteins for biochemical, biophysical, and functional assays. Human plasma samples, collected as described previously, were also processed for LDL isolation. Briefly, very low-density lipoproteins (VLDLs) were first discarded after spinning plasma at 36,000 rpm for 18 h at 4 °C using a fixed-angle rotor (50.2 Ti, Beckman) mounted on an Optima L100 XP ultracentrifuge (Beckman). Subsequently, VLDL-free plasma was layered with 1.063 g/mL KBr solution and centrifuged at 36,000 rpm for 18 h at 4 °C. KBr solution was finally added to VLDL and LDL-free plasma to isolate HDL (d1.063–d1.210 g/mL). LDLs and HDLs were dialyzed against 0.02M Trizma, 0.15M NaCl, 1 mM EDTA, pH 7.5 for 18 h, and then against normal saline for 2 h. Lipoproteins were filter-sterilized (0.22 μm Millex-GV filter unit, Millipore). Protein concentrations were determined using the BCA protein assay (Thermo Scientific), and the cholesterol concentration, with a commercial kit (IL test Cholesterol, Izasa).

2.12.2. Study of passive and sphingomyelinase (SMase)-induced LDL aggregation

LDL (1.44 mg/mL) isolated from the different experimental groups was left 37 °C or incubated with 40 U/L of Bacillus cereus SMase (Sigma-Aldrich, Schnelldorf, Germany) at 37 °C for increased time periods (24, 48 and 120 h) as previously described [18].

LDL lipolysis was halted by the addition of EDTA to a final concentration of 10 mM. Turbidity of murine and human samples, indicative of LDL aggregation, was assessed by measuring the absorbance of 100 μL of LDLs (1.44 mg/mL ApoB) in 96-well microplates at 405 nm. For human samples, turbidity measurements were further validated by evaluating particle size distribution (PSD) using dynamic light scattering (DLS).

2.12.3. Particle size distribution (PSD) measuraments in human LDL samples from patients with familial hypercholesterolemia

The PSD analysis was was performed using a Zetasizer Nano ZS (Malvern Panalytical, UK) with square polystyrene cuvettes (DTS0012), at a scattering angle of 173° and a temperature of 25 °C. LDL samples from the SMase-induced aggregation assay were diluted 50 times in PBS 1X for native LDL and 100 times for LDL incubated with SMase, as these were determined to be the most appropriate dilution factors. Each sample was measured in triplicate, and the z-average value was used for statistical analysis.

2.12.4. Study of proteoglycan (PG)-induced LDL aggregation

LDL isolated from the three study groups was mixed with chondroitin sulfate proteoglycans (CSPGs) (Merck, CC117). The interaction between CSPGs and LDL was conducted after equilibrating LDL and CSPGs in a solution containing 5 mmol/L HEPES, 20 mmol/L NaCl, 4 mmol/L $CaCl_2$, and 2 mmol/L $MgCl_2$, pH 7.2. LDL and CSPGs were incubated at a protein ratio of 100:1 for various time intervals at 37 °C, as previously described by our group [6].

2.12.5. High-performance thin layer chromatography (HPTLC) of phospholipid lipid content in murine and human LDL samples

LDL (6 μg for mouse samples and 9 μg for human samples) was lipid-extracted using organic solvents, following a previously described protocol by our group with minimal modifications [10]. Samples were then applied to horizontal, one-dimensional high-performance thin-layer chromatography (HPTLC) plates (Merck, HPTLC Silica Gel 60, 1.05641.0001). Phospholipids were separated on HPTLC using a solvent system consisting of chloroform ethil acetate: acetone:isopropanol: ethanol:methanol:water:acetic acid (30:6:6:6:16:28:6:2). The separated phospholipids were visualized by staining with a solution containing

7.5 % (w/v) acetate, 2.5 % (w/v) $CuSO_4$, and 8 % (v/v) H_3PO_4 in water. A mixture of phospholipids (Sigma, Ref pH-7) was run as standards. The spots corresponding to different phospholipids were quantified by densitometry against the standard curve using a GS-800 Calibrated Densitometer (Bio-Rad).

2.12.6. Agarose gel electrophoresis of murine and human LDL

VLDL, LDL, and HDL lipoproteins (2 μL) were electrophoresed on 0.66 % agarose gels at 65 V for 1h followed by 90 V for 20 min as previously described [18]. Fixed gels were dehydrated and stained with Coomassie Blue. Decolored gels were captured with the Bio-Rad GS-800 scanner.

2.12.7. Z-potential measurements to identify changes in LDL particle charge induced by DP3 binding

Z-Potential was measured using Zetasizer Nano ZS equipment (Malvern Panalytical, UK). The analysis was performed using the capillary cell (DTS1070), the scattering angle of 12° and a temperature of 25 °C. LDL samples were diluted 50 times in Q1 water and each sample was measured three times taking the average value for the statistical analysis.

2.12.8. Transmission electron microscopy (TEM) of murine LDL samples

TEM was performed using an H-7000 microscope (Hitachi, Japan) with an acceleration voltage of 75 kV. For the analysis, LDL samples were placed on a TEM grid and allowed to settle for 1 min before blotting. The grid was then stained with 2 % uranyl acetate for 1 min, after which the excess stain was gently removed using Whatman filter paper. The particle diameters of LDL from the TEM images were quantified using the line tool in ImageJ (v1.54 COQ) to measure length. Subsequently, for each condition (with or without SMase), size distributions were stratified and compared between groups.

2.12.9. Circular Dichroism of murine LDL to identify conformational ApoB100 changes induced by peptides

To assess changes in the conformation of ApoB100, Circular Dichroism (CD) spectra of native and modified LDLs (0.02 mg of protein/mL) in 10 mM phosphate buffer were obtained using a Jasco J-815 spectropolarimeter (MD, USA) with a 1 cm quartz cuvette at 25 °C. Spectra were recorded over the range of 190–260 nm, with measurements taken at 0.5 nm intervals, a scan rate of 50 nm/min, and a bandwidth of 1 nm. Data were processed by subtracting the background and applying baseline correction. Results were expressed in terms of mean residue molar ellipticity ($[\theta]_{MRW}$) in units of degree cm^2 $dmol^{-1}$. The helix fraction (FH) was calculated using the slope method in the 230–240 nm region as described by Wei et al. [31]. Briefly, the slope (A) of the CD spectra in the 230–240 nm range was calculated for each sample, and the related helix fraction (FH) was determined using the equation: $FH = mA + B$, where m is 5.14×10^{-3} and B is 2.97×10^{-3} [31].

2.12.10. SDS-PAGE and Western blot analysis of murine LDL

ApoB100 was detected by Western blot analysis following the electrophoresis of LDL on 6 % SDS-PAGE gels. Nitrocellulose membranes were incubated with anti-ApoB100 polyclonal antibodies (Roche Diagnostics S.L., Ref: 3032574122, polyclonal anti-human ApoB-100, dilution 1:5000) for O/N at 4 °C. After several washes, the membranes were incubated with secondary anti-sheep antibodies (dilution 1:10000, Dako; Glostrup, Denmark). Bands were visualized using the ECL Prime Western Blotting Detection Reagent (Amersham) and quantified by densitometry with a ChemiDoc system and Quantity One software (Bio-Rad, Hercules, CA, USA). The results are expressed as arbitrary units of intensity. These anti-ApoB100 polyclonal antibodies specifically recognize the ApoB100 isoform in the immunoturbidimetry assay, as they do not recognize ApoB in chylomicrons or mouse serum from $Ldlr^{-/-}$ mice, ensuring they do not detect ApoB48 (human or murine) by immunoturbidimetry. However, the specificity of this antibody for ApoB100 in Western blot analysis cannot be fully ensured.

2.13. Statistical analysis

All results are shown as mean ± standard deviation (SD). Statistical analysis was performed using Prism software (version 9.0, GraphPad). For all variables, normal distribution was tested using the Shapiro-Wilk normality test. The Kruskal-Wallis test, followed by Dunn test was used when one or more groups did not show Gaussian distribution. For comparison of two groups, the unpaired 2-tailed Student's *t*-test (for unequal variances) or two-way ANOVA followed by Tukey's post hoc test (normality and variance homogeneity) was used. Differences were considered to be statistically significant when $p < 0.05$.

3. Results

3.1. Characterization of lipid and lipoprotein profile of $Ldlr^{-/-}$ *hApoB100* mice

The humanized ApoB100 Tg mice (*$Ldlr^{-/-}$ hApoB100*) was generated as described in online Fig. S1 and validated through the characterization of its lipid and lipoprotein profile by molecular, biochemical, and biophysical approaches. Polyacrylamide gradient gel electrophoresis performed with VLDL, LDL, and HDL isolated from the blood of *$Ldlr^{-/-}$* and *$Ldlr^{-/-}$ hApoB100* mice models revealed differences in the distribution of ApoB isoforms. Gradient gels (Fig. 1A and B) revealed that in *$Ldlr^{-/-}$* mice, VLDL carried the majority of total apoB100 (84.87 ± 0.75 %) and apoB48 (81.81 ± 4.35 %). This distribution changes in *$Ldlr^{-/-}$ hApoB100* mice, where LDL carried the bulk of the extremely high levels of apoB100 (88.81 ± 2.35 %), while the moderate total apoB48 levels were nearly equally distributed between VLDL (39.15 ± 9.39 %) and LDL (38.74 ± 2.26 %). In the LDL of this humanized model, apoB100 represents 87.83 ± 0.74 % of the total apoB, while apoB48 accounts for only 12 ± 0.74 %. Western blot analysis confirmed a substantial increase in the ApoB100 content of LDL in *$Ldlr^{-/-}$ hApoB100* mice compared to *$Ldlr^{-/-}$* mice (online Fig. S3). Notably, ApoB48, the predominant isoform in LDL of *$Ldlr^{-/-}$* mice, exhibited a much higher tendency to aggregate compared to LDL from the humanized murine model or humans (online Fig. S4A). While sphingomyelinase (SMase) effectively increased LDL aggregation in the humanized murine model, as in humans, it did not further enhance the passive LDL aggregation observed in *$Ldlr^{-/-}$* mice (online Fig. S4B). Immunoturbidimetry assays also validated a significant increase in ApoB100 levels in *$Ldlr^{-/-}$ hApoB100* mice compared to *$Ldlr^{-/-}$* mice, with notable increases in total serum ($p < 0.001$), VLDL ($p < 0.001$), and especially in LDL ($p < 0.001$) (Table 1). Cholesterol content was strongly increased in LDL from *$Ldlr^{-/-}$ hApoB100* compared to that from *$Ldlr^{-/-}$* mice (Fig. 1C). Serum total cholesterol and triglyceride (TG) levels were also significantly increased in the humanized Tg mice (Table 1). There were no significant differences in the body weight between *$Ldlr^{-/-}$ hApoB100* and *$Ldlr^{-/-}$* mice ($p = 0.823$) (Table 1). Taken together, these results support *$Ldlr^{-/-}$ hApoB100* mice as a humanized experimental model of hypercholesterolemia.

3.2. Imaging monitoring of TAMRA-DP3 biodistribution in $Ldlr^{-/-}$ *hApoB100 mice*

To quantify the peptide biodistribution and changes over time in the different organs of the living mice, we used tail vein intravenous injection (7.14 mL/kg) of TAMRA-DP3 (50 mg/kg) in *$Ldlr^{-/-}$ hApoB100* female mice, with posterior bioimaging using the IVIS at 15′, 30′ and 60′ post-injection (Fig. 2A). Immediately after mice sacrifice (at 15, 30 and 60' post-injection), we performed *ex vivo* wide-field imaging, defined as ROI (region of interest), of the whole organ. As a control for basal fluorescence, we also imaged organs from untreated mice with no

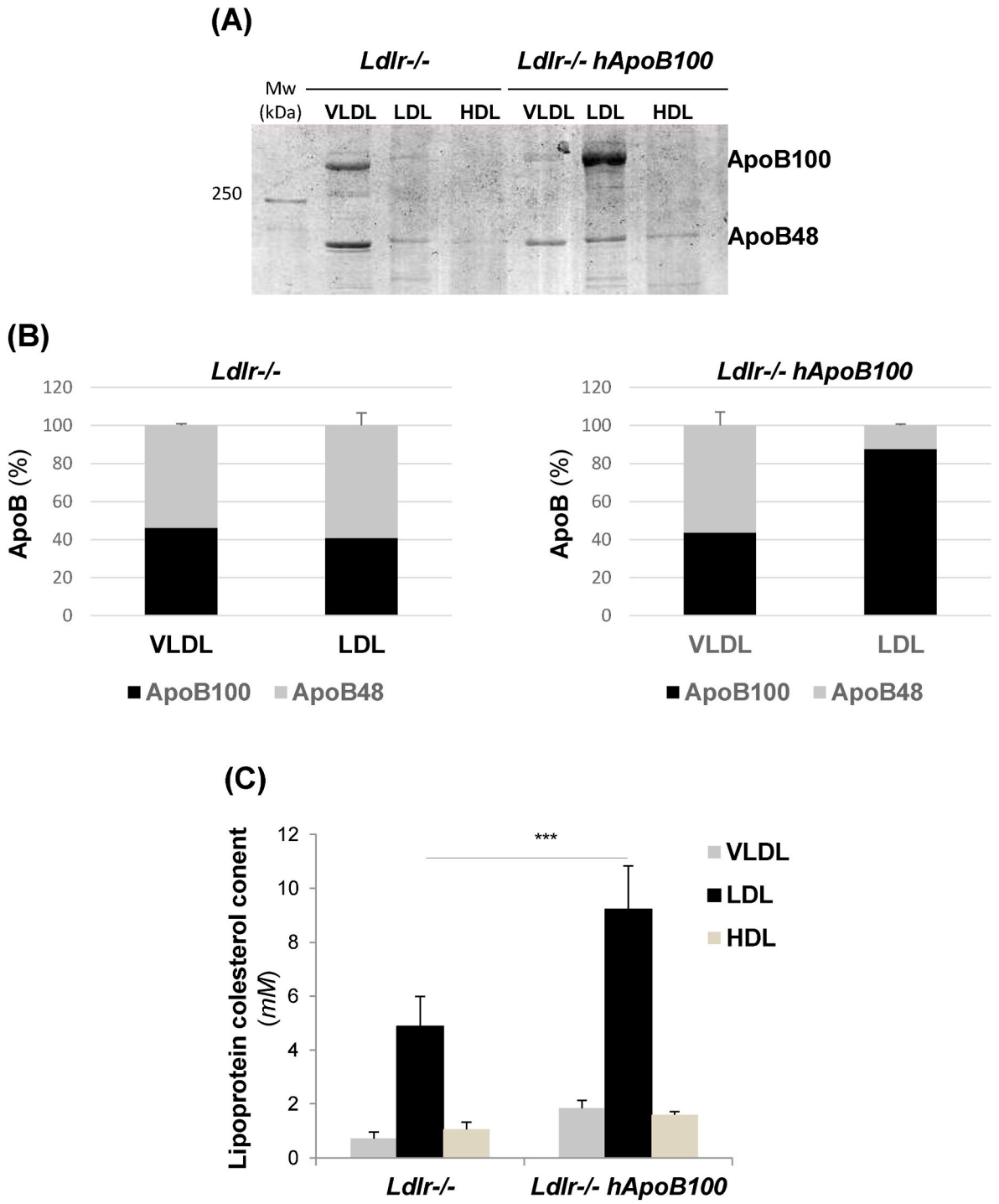

Fig. 1. Comparison of lipoprotein profiles of *Ldlr−/−* and *Ldlr−/− hApoB100* mice models.
(A,B) Representative polyacrylamide gradient gel electrophoresis and bar graphs illustrating the percentage of ApoB100 and ApoB48 in VLDL and LDL fractions from $Ldlr^{-/-}$ (left panel) and $Ldlr^{-/-}$ *hApoB100* (right panel) mice models. (C) Bar graphs depicting the quantification of cholesterol content in VLDL, LDL, and HDL fractions from both $Ldlr^{-/-}$ and $Ldlr^{-/-}$ *hApoB100* mice models. Data are presented as mean ± SD from 3 pools per group (3 mice per pool, n = 9/group). Statistical significance was determined using Student's t-test for independent samples. ***$p < 0.001$ compared to $Ldlr^{-/-}$ mice.

fluorescence injection and subtracted these values from those obtained for the respective organ in the experimental groups. After the kidney (Fig. 2B), the liver and heart showed the highest fluorescence intensity at 15-min post DP3 injection, which remained high at 30-min post-injection (Fig. 2C). In the aorta and brain, a transient increment of fluorescence was observed at 15-min post-injection (Fig. 2C).

In agreement with FLI results, confocal microscopy confirmed the excretion of TAMRA-DP3 (in red) by the kidney of $Ldlr^{-/-}$ *hApoB100* mice (Fig. 2D). Further, using confocal microscopy, we observed the arrival of TAMRA-DP3 (in red) to the atherosclerotic lesions of the arterial intima in aortic proximal sections where ApoB100 (in green) show a high degree of colocalization (yellow) with the peptide in the arterial intima (Fig. 2E).

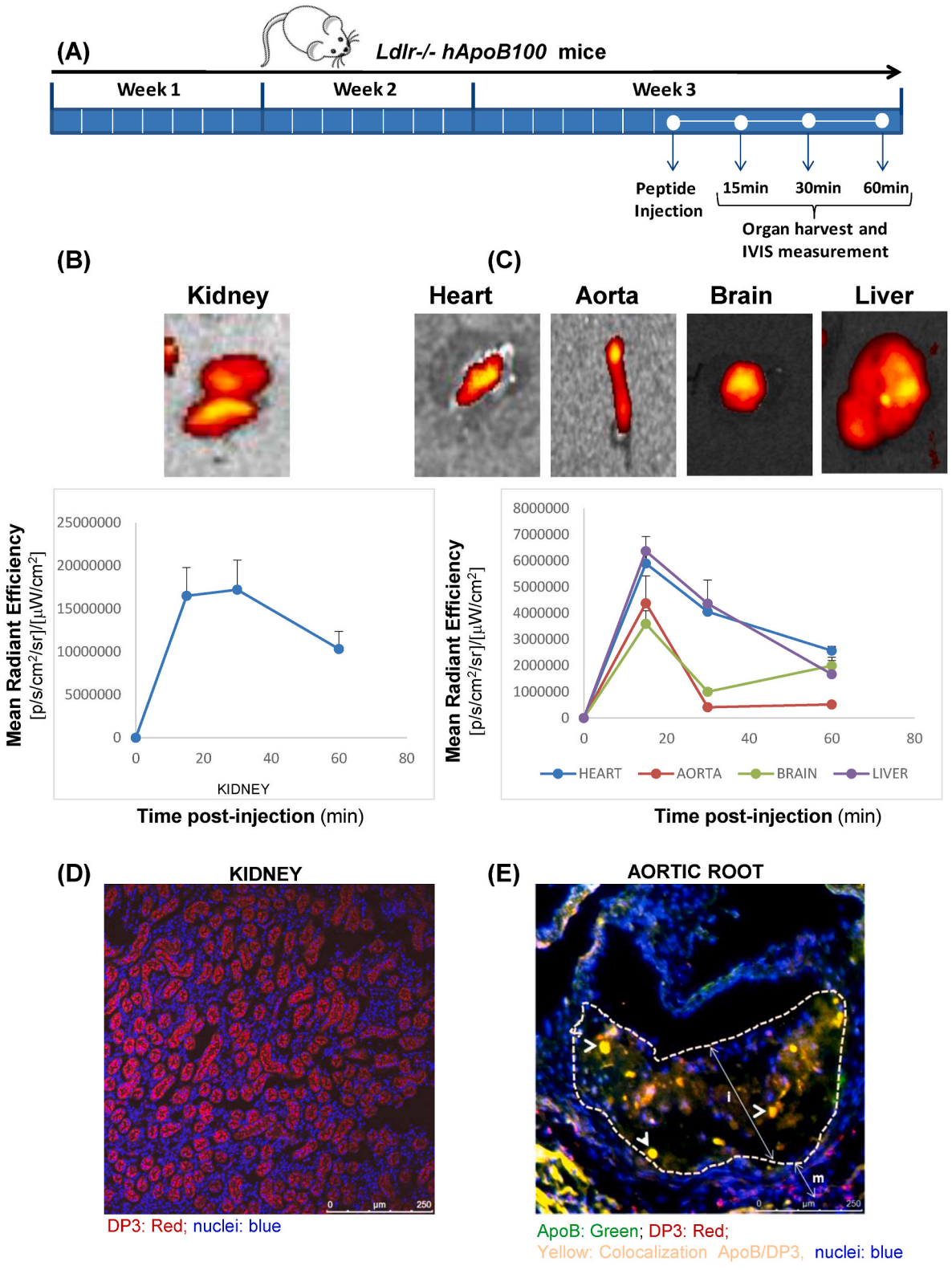

Fig. 2. Biodistribution of TAMRA-DP3 in *Ldlr*$^{-/-}$ *hApob100* mice.
(A) Representative scheme of the experimental procedure for biodistribution studies. (B, C) Representative *ex-vivo* images of the maximal DP3 fluorescence detected in peripheral tissues and line graphs showing the time course evolution of TAMRA-DP3 fluorescence detected in kidney and peripheral organs (heart, aorta, brain and liver). Data represent the mean ± SD of DP3 fluorescence determinations (n = 3/group). (D, E) Representative confocal microscopy images showing the high presence of TAMRA-DP3 (red) in the kidney glomerulus, which is the main renal filtering unit, and the high presence of TAMRA-DP3 (red) and ApoB100 (green) in the arterial intima (i) of an atherosclerotic plaque with a serious intimal (i)-media (m) thickening. Arrows show the high degree of colocalization (yellow) between DP3 and ApoB100 in the arterial intima of the aortic root. n, nuclei (blue). (For interpretation of the references to color in this figure legend, the reader is referred to the Web version of this article.)

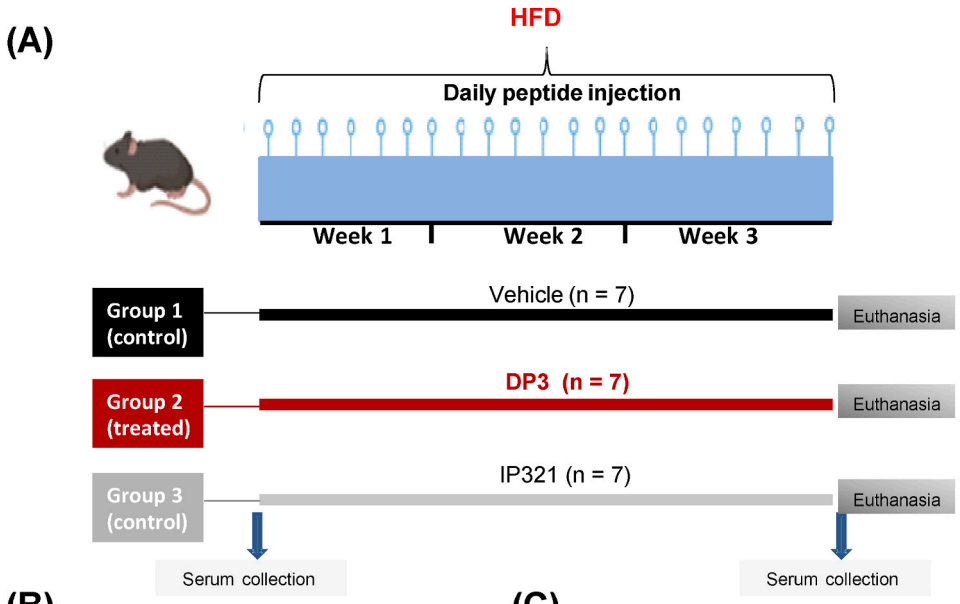

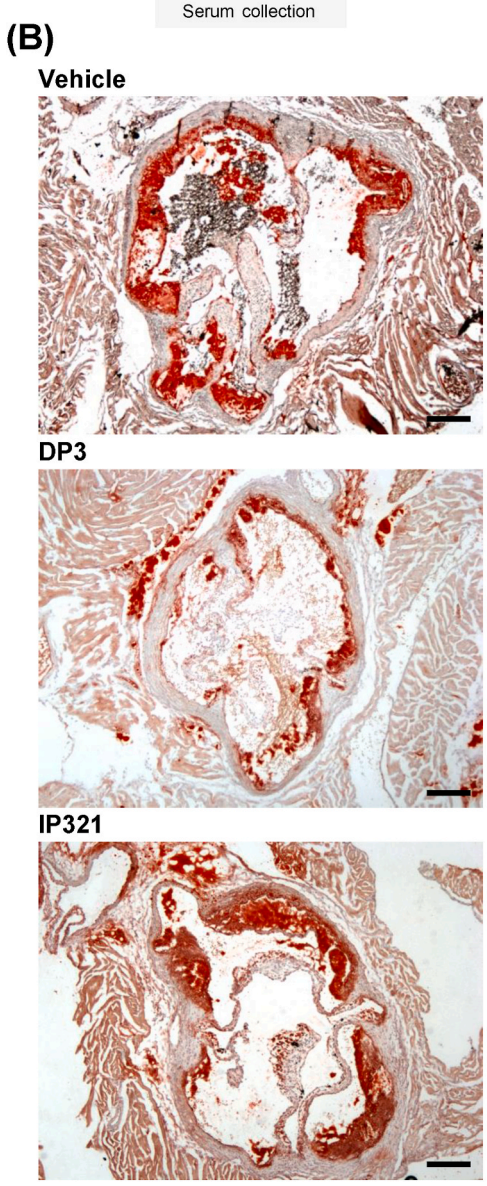

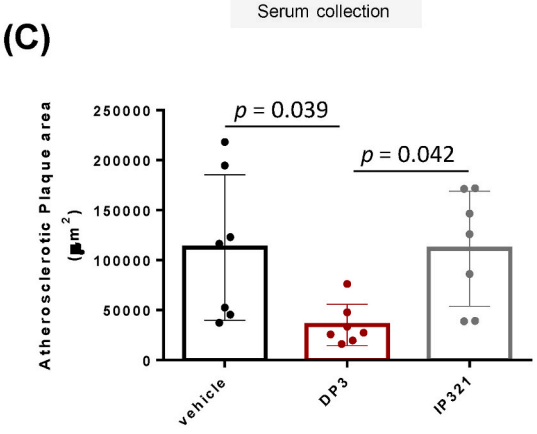

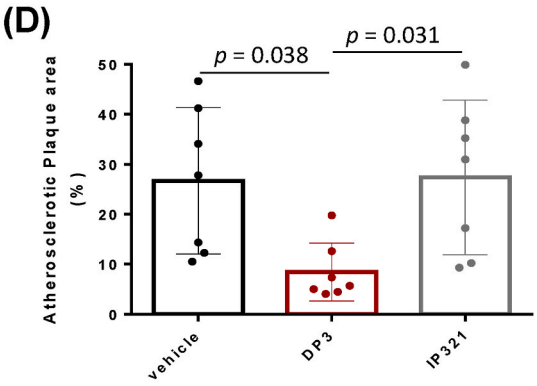

(caption on next page)

Fig. 3. Decreased intimal neutral lipid accumulation in *Ldlr*$^{-/-}$ *hApob100* mice treated with the DP3 peptide.
(A) Representative scheme of groups and experimental procedure set up to analyze the effect of DP3 on HFD-induced atherosclerosis. Mice were fed an HFD for 3 weeks starting at 8 weeks and daily injected positive peptide (DP3) (treated group), negative peptide (IP321) or vehicle as control groups. (B) Immunohistochemical representative images of oil red O–stained aortic root sections showing atherosclerotic plaques in *Ldlr*$^{-/-}$ *hApob*100 Tg mice. Scale bar, 200 μm. Quantification of aortic lipid accumulation was performed in serial cross-sections (7 μm) at the beginning and in the middle of the aortic valve. Results are shown as total oil red O–stained area (C) or as percentage of total aortic root area (D). Data represent the mean ± SD. (n = 7/group). Differences between groups were analyzed using Student's *t*-test for independent samples. (For interpretation of the references to color in this figure legend, the reader is referred to the Web version of this article.)

3.3. Effects of DP3 in HFD-induced vascular lipid accumulation in *Ldlr*$^{-/-}$ *hApoB100* mice

During the three weeks of HFD dietetic intervention, mice was daily treated with DP3 or IP321 peptide, or with vehicle, as depicted in Fig. 3A. HFD (0.2 % cholesterol, 3 weeks) increased circulating cholesterol levels in serum ($p < 0.001$) and LDL ($p < 0.001$), and it also increased ApoB100 levels (g/L) in serum ($p < 0.001$) and LDL ($p < 0.001$), however, serum TG levels were not altered by this diet ($p = 0.950$) (Table 2). There were no differences in the upregulatory effect of HFD in serum/LDL cholesterol, apoB, or serum triglyceride circulating levels between the three tested groups (Table 2).

The imaging and analysis of HFD-induced vascular lipid accumulation was performed in Oil Red O-stained aortic root cross-sections as detailed in Methods. There was a significant reduction in the aortic root atherosclerotic plaque area in the DP3-treated group compared to control groups (vehicle, $p = 0.039$ or IP321, $p = 0.042$) (Fig. 3B and 3C). The percentage of positive lipid area *versus* total aortic root area was also significantly lower in DP3 compared to vehicle ($p = 0.038$) and to IP321 ($p = 0.031$) control groups (Fig. 3B and D).

3.4. Effect of peptide administration in systemic and hepatic inflammation

To assess the effect of peptide administration on systemic inflammation, we analyzed the number of peripheral monocytes in the blood from the three mouse groups. Flow cytometry revealed no significant differences in blood monocyte counts between the DP3-treated and control groups (DP3: $4.67 \times 10^{-2} \pm 0.022$ *vs.* vehicle: $5.97 \times 10^{-2} \pm 0.014$, $p = 0.793$, and *vs.* IP321: $6.65 \times 10^{-2} \pm 0.058$, $p = 0.711$). Real-time PCR analysis indicated that peptide administration had no effect on the expression of hepatic pro-inflammatory mediators, including CD36, TNFα, CD68, and CCL-2 (online Fig. S5). Additionally, thin-layer chromatography of hepatic lipid extracts showed no differences in CE, TG, or FC content between the groups (online Fig. S6).

3.5. Susceptibility of LDL isolated from DP3-treated (compared to that from control groups) to passive (no SMase) and SMase-induced LDL aggregation

Biochemical studies showed no differences in cholesterol and ApoB100 content of LDL isolated from the three mice groups (Table 2). However, time-course turbidity assays showed that LDL isolated from DP3-treated group was more resistant to passive (Fig. 4A, left panel) and SMase-induced aggregation (Fig. 4A, right panel) than control groups (vehicle and IP321). In line, agarose gels showed that sphingomyelinase (SMase) induced a smeared aggregation pattern of LDL from vehicle and IP321 control groups that was not present in LDL from DP3-treated mice (Fig. 4B).

TEM images of LDL size distribution revealed that, in the absence of SMase, LDL from the DP3-treated group predominantly consisted of individual LDL particles, whereas LDL from the control and IP321 groups exhibited a more heterogeneous particle size distribution, including small LDL aggregates (Fig. 4C and D, upper panels, and online Fig. S12A). Upon exposure to SMase, LDL aggregates were observed in the control groups (vehicle and IP321), but they were almost absent in the LDL from the DP3-treated group (Fig. 4C and D, lower panels, and online Fig. S12B). Turbidity assays showed no differences in VLDL isolated from the different groups, either in the absence or presence of SMase (online Fig. S7). DP3 did not affect LDL aggregation induced by proteoglycans, as proteoglycans strongly and rapidly induced LDL aggregation regardless of the LDL tested, at least under our experimental conditions (online Fig. S8).

Table 1
Serum lipids in *Ldlr*$^{-/-}$ *hApoB100* compared to *Ldlr*$^{-/-}$ female mice on a regular chow diet.

Strain	*Ldlr*$^{-/-}$	*Ldlr*$^{-/-}$ *hApoB100*	*p*
Body weight (g)	24.17 ± 2.70	22.50 ± 0.78	0.823
Total cholesterol (mM)	7.61 ± 0.97	15.99 ± 1.96	<0.001
Total triglycerides (mM)	2.68 ± 0.75	6.04 ± 0.82	<0.001
Total ApoB100 (g/L)	0.00 ± 0.00	2.35 ± 0.47	<0.001
VLDL ApoB100 (g/L)	0.00 ± 0.00	0.13 ± 0.03	<0.001
LDL ApoB100 (g/L)	0.03 ± 0.01	1.66 ± 0.26	<0.001

Six and five serum pools (3 animals/pool) (n = 18/group and n = 15/group) were used for determinations in *Ldlr*$^{-/-}$ *hApoB100* and *Ldlr*$^{-/-}$ female mice. Data are expressed as mean ± SD.*$p < 0.001$ *Ldlr*$^{-/-}$ *hApoB100 vs. Ldlr*$^{-/-}$ mice.

Table 2
Biochemical variables of *Ldlr*$^{-/-}$ *hApoB100* female mice from the 3 groups (vehicle, DP3 and IP321 groups) at the pre-diet time and after 3 weeks feeding on a high fat diet (0.2 % cholesterol).

	vehicle	DP3	IP321	vehicle	DP3	IP321
	Pre-diet	Pre-diet	Pre-diet	Post-diet	Post-diet	Post-diet
Body weight (g)	22.83 ± 1.87	23.01 ± 2.51	21.95 ± 1.23	23.44 ± 2.88	23.29 ± 2.19	23.34 ± 3.32
Cholesterol (mM)	13.40 ± 2.23	15.06 ± 1.68	14.45 ± 1.58	36.12 ± 3.26*	40.18 ± 2.01*	36.66 ± 4.89*
Triglycerides (mM)	4.41 ± 1.64	6.14 ± 1.12	5.38 ± 1.69	4.00 ± 1.16	5.41 ± 3.44	5.62 ± 3.03
ApoB100 (g/L)	2.21 ± 0.29	2.62 ± 0.27	2.24 ± 0.47	3.11 ± 0.55*	3.37 ± 0.42*	3.58 ± 0.49*
LDL-chol (mM)	7.30 ± 0.96	8.91 ± 2.07	7.41 ± 2.19	22.31 ± 3.00*	24.41 ± 3.57*	23.86 ± 2.54*

Six serum pools (3 animals/pool) (n = 18/group) were used for determinations. Data are expressed as mean ± SD. *$p < 0.05$ post-diet versus pre-diet for each group.

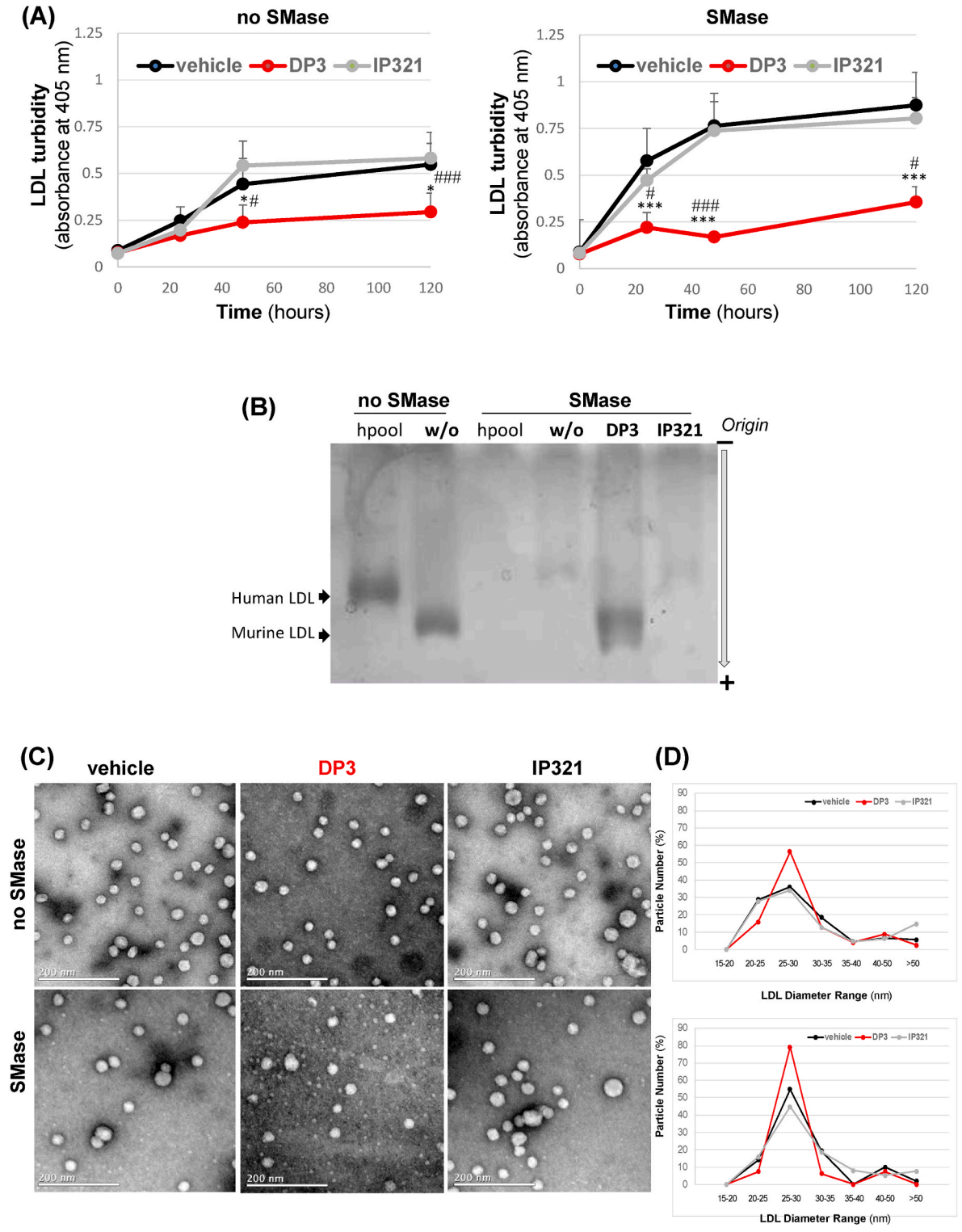

Fig. 4. Passive and SMase-induced LDL aggregation is reduced in LDL from DP3-treated mice compared to control (vehicle and IP321) groups.
(A) Line graphs showing LDL aggregation monitored at increasing times by turbidity (absorbance at 405 nm). Turbidity was measured at 37 °C without exposure of LDL to SMase (passive aggregation) or with exposure of LDL to SMase (40 U/L) at the tested times. LDL was used at 1.44 mg/mL ApoB. Data represent the mean ± SD of 3 pools per group. 3 mice/pool, n = 9/group. *$p < 0.05$ and ***$p < 0.005$ for DP3-treated *versus* vehicle control group. #$p < 0.05$ and ###$p < 0.005$ for DP3-treated *versus* IP321 control group. Differences between groups were analyzed using Student's *t*-test for independent samples. (B) Representative agarose gels comparing the electrophoretic mobility pattern of LDL isolated from the different experimental groups and exposed to SMase (40 U/L) for 24 h. LDL isolated from a human pool is also shown as reference (human LDL). w/o = vehicle. (C) Representative TEM images showing LDL size and morphology (unexposed, upper panels, or exposed to Smase, 40 U/L, 24 h, lower panels) from DP3-treated *versus* control (vehicle and IP321) groups. (D) Graphs showing the LDL particle size distribution, depicting the percentage of particles within each diameter range relative to the total particle count in each TEM image. Results are shown as mean of 2–3 pools per group (3 mice/pool, n = 6–9/group).

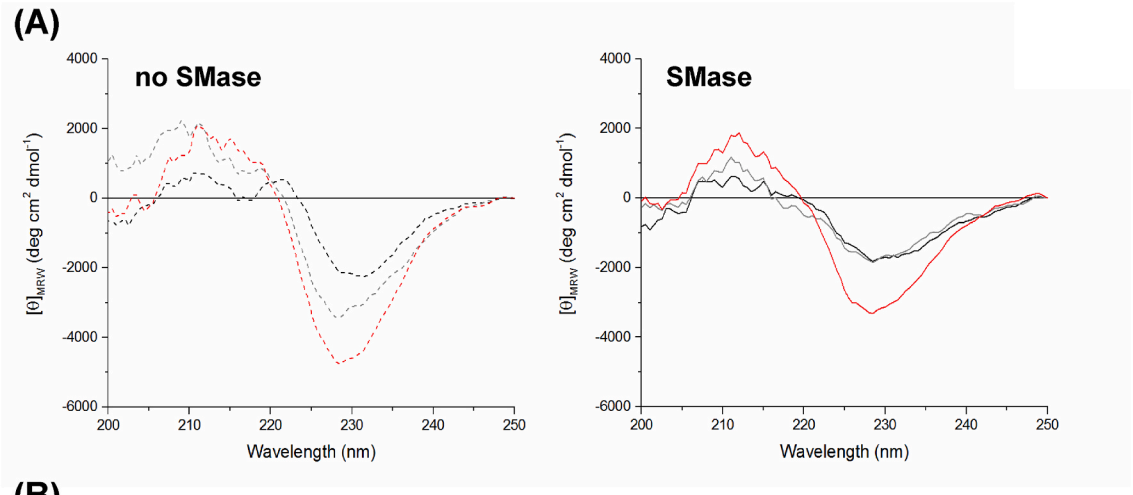

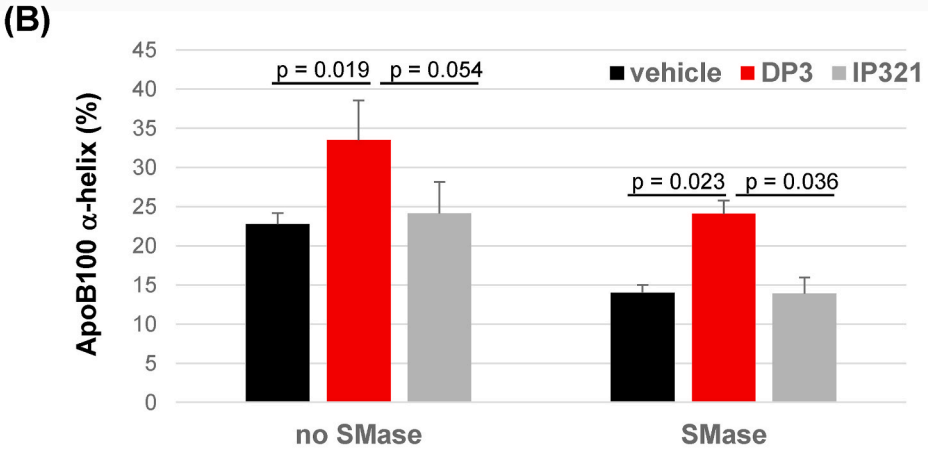

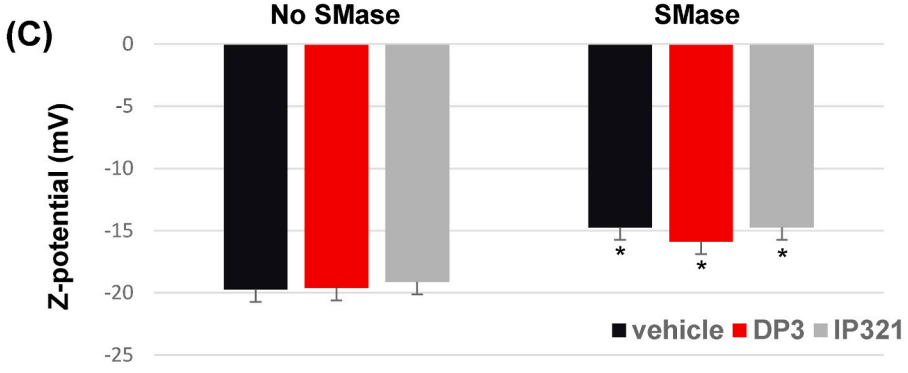

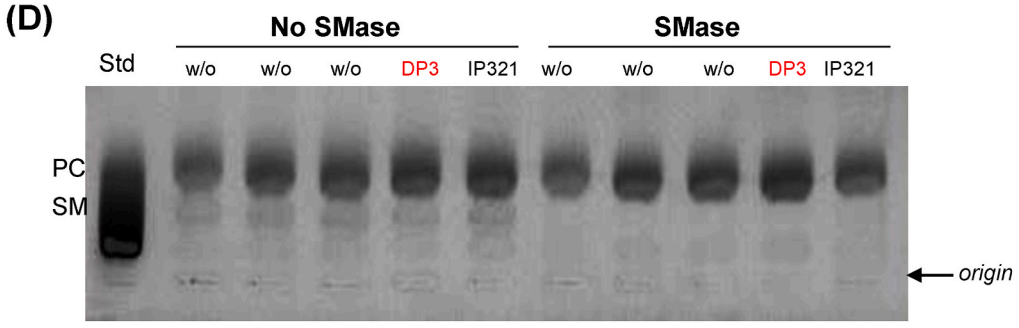

(caption on next page)

Fig. 5. DP3 Stabilizes ApoB100 conformation by increasing α-helix content without altering the net charge of LDL.
(A, B) Circular dichroism (CD) spectra of LDL samples (0.02 mg/mL) isolated from experimental groups, either unexposed to SMase or exposed to SMase (40 U/L). CD spectra were acquired in the range of 190–260 nm with 0.5 nm intervals, a 50 nm/min scan rate, and a 1 nm bandwidth. The fraction of α-helix was calculated using the 230–240 nm slope method, as described in the Methods section. (C) Zeta potential (Z-potential) measurements of LDL samples (0.012 mg/mL) performed with a Zetasizer Nano ZS equipment to detect alterations in LDL charge. Data are presented as mean ± SD of 2–3 pools per group (3 mice/pool, n = 6–9/group). Differences between groups were analyzed using Student's t-test for independent samples. (D) Representative high-performance thin layer chromatography (HPTLC) analysis of LDL phospholipid content. Phosphatidylcholine (PC) and sphingomyelin (SM) are indicated, with standards (Std) shown for comparison.

3.6. Effect of DP3 on ApoB100 structural conformation in LDL

Circular Dichroism (CD) spectra indicated that ApoB100 in LDL from DP3-treated mice had an increased percentage of α-helix secondary structures compared to ApoB100 in LDL from control groups (DP3: 33.52 ± 5.05 % vs. vehicle: 22.79 ± 1.41 %, p = 0.016; vs. IP321: 24.16 ± 3.96 %, p = 0.054) (Fig. 5A, left panel, and 5B). SMase exposure caused a significant loss in the percentage of ApoB100 α-helix structures in LDL from control groups (vehicle: 14.00 ± 0.99 %; IP321: 13.93 ± 2.03 %), while a percentage of α-helix structures comparable to that in SMase-unexposed LDL was maintained in LDL of DP3-treated group (24.09 ± 1.71 %) (Fig. 5A, right panel, and 5B). Western blot analysis further supported the conformational stabilization of ApoB100 by DP3, as evidenced by reduced exposure of reactive ApoB100 epitopes to anti-ApoB100 antibodies (online Fig. S9). Another indicator of the stable conformation of ApoB100 in LDL induced by DP3 was that DP3 did not interfere with the binding of LDL to the LDL receptor. Neither DP3 nor IP321 influenced the effect of native LDL on intracellular CE/FC content in smooth muscle cells. However, DP3, but not IP321, significantly reduced the increased intracellular CE/FC ratio induced by exposure to SMase-LDL (online Fig. S10). These results suggest that DP3 specifically reduces the uptake of aggregated LDL without altering the uptake of native LDL.

Previous studies from our group have demonstrated that DP3 binds to the 3227-IKFDKYKAEK-3236 epitope located in the C-terminal region of ApoB-100 [18]. To determine whether DP3 alters the charge of LDL particles, we measured the Z-potential of LDL using a Zetasizer Nano ZS. The results showed that neither DP3 nor IP321 altered the charge of ApoB100 in murine LDL, whether unexposed (Fig. 5C, left) or exposed to SMase (Fig. 5C, right). Consistent with this, agarose gel electrophoresis revealed no changes in the electrophoretic mobility of LDL from the different groups (online Fig. S11). However, exposure of LDL from all three mouse groups to SMase caused a significant change in particle Z-potential, indicating a net change in the charge of LDL particles. High-performance thin-layer chromatography (HPTLC) analysis of LDL phospholipid content revealed that the sphingomyelin (SM) content in murine LDL is quite low, and that was completely depleted by SMase in LDL independently of the group (Fig. 5D).

3.7. Effects of DP3 ex-vivo on human LDL tendency to aggregation. Studies in LDL isolated from patients with familiar hypercholesterolemia (HF)

The efficacy of DP3 to preserve human LDL integrity *ex-vivo* was tested on LDL isolated from patients with primary familiar hypercholesterolemia. The main altered variables in this group of patients were increased total cholesterol (357.62 ± 59.55 mg/dL) and LDL cholesterol levels (271.46 ± 51.07 mg/dL) (online Table S1). SMase-induced LDL turbidity was almost completely abolished in DP3 but not in IP321-exposed LDL from all patients with FH (Fig. 6A).

These findings were further validated by measurements of LDL particle size distribution using Dynamic Light Scattering (DLS). Similar to the results from turbidity assays, DLS studies showed that in the presence of SMase, DP3 preserved the Z-average LDL size, maintaining it at levels comparable to those of SMase-unexposed LDL (Fig. 6B). Additionally, agarose gel electrophoresis demonstrated that DP3, but not IP321, effectively recovered the SMase-induced loss of bands (which is attributed to the exclusion of the largest LDL aggregates by the pore size of the agarose gels) in human LDL samples (Fig. 6C).

HPTLC analysis revealed that L-α-PC levels in human LDL were unaffected by SMase treatment (Fig. 6D and E), while SM was completely removed from LDL following SMase exposure (Fig. 6D and F). Notably, DP3, but not IP321, effectively protected LDL-SM against SMase-induced degradation in these human LDL samples (Fig. 6D and F).

4. Discussion

In the present study, we show that DP3 contributes to inhibit atherosclerosis *in vivo* through inhibition of LDL aggregation, an effect primarily caused by preservation of structural ApoB100 conformation in the LDL of a humanized ApoB100 hypercholesterolemic murine model. We also show that DP3 shows efficacy *ex-vivo* to maintain the integrity of LDL isolated from patients with familial hypercholesterolemia.

Murine models have serious limitations for testing the efficacy of new anti-atherosclerotic compounds targeting lipoproteins since in mice, differently to humans, cholesterol is mostly transported by HDL [32,33]. In addition, the main isoform of ApoB present in the murine lipoproteins is ApoB48, not ApoB100 as in humans. Here, we developed a new transgenic murine model that overexpresses human ApoB100 in the background of Ldlr deficiency (*Ldlr*$^{-/-}$ *hApoB100*). Polyacrylamide gradient gel electrophoresis revealed that in *Ldlr*$^{-/-}$ *hApoB100* mice, differently that in *Ldlr*$^{-/-}$, ApoB100 is mainly carried by LDL and represents almost the 88 % of the total ApoB present in this lipoprotein, while ApoB48 accounts for only 12 %. Our comparative studies of LDL isolated from *Ldlr*$^{-/-}$, *Ldlr*$^{-/-}$ *hApoB100* mice, and humans revealed that, unlike human LDL, which remains stable over long time periods, murine LDL undergoes passive aggregation at short time post-isolation. This passive aggregation occurs more rapidly and to a greater extent in LDL from *Ldlr*$^{-/-}$ mice (which contain 60 % ApoB48) than in LDL from *Ldlr*$^{-/-}$*hApoB100* mice (which contain 12 % ApoB48). These results are in line with previous studies highlighting the influence of ApoB48 on LDL aggregation [34,35]. Thus, although present in lower proportions, ApoB48 in LDL from *Ldlr*$^{-/-}$ *hApoB100* mice may contribute to increased tendency for passive aggregation and more limited efficacy of DP3 in preventing LDL aggregation in murine models compared to humans. Despite these particular differences, according to our results, LDL from *Ldlr*$^{-/-}$ *hApoB100* mice exhibits a similar pattern of SMase-induced aggregation than humans. In addition, human ApoB100 overexpression *per se* raises cholesterol levels in serum, which is mainly carried by LDLs in this humanized murine model. One plausible mechanism underlying upregulatory effects of ApoB100 overexpression in blood cholesterol levels is the critical role of ApoB100, along with microsomal triglyceride transfer protein (Mttp), in the production of VLDL particles by the liver [36,37]. The levels of LDL cholesterol (9.37 ± 2.30 mM, 360 mg/dL) and LDL-associated hApoB100 (1.26 ± 0.09 g/L) in the *Ldlr*$^{-/-}$ *hApoB100* mice are in the range of those reported in homozygous familial hypercholesterolemic patients [37,38]. In fact, *Ldlr*$^{-/-}$ *hApoB100* mice has been proposed as a promising model to study new therapeutic approaches useful for human familial hypercholesterolemia [39,40]. Thus, the humanized lipoprotein profile makes hApoB100 Tg mice a suitable model for testing the efficacy of the peptide DP3 on atherosclerosis as well as for determining lipoprotein-related mechanisms involved.

Previous studies from our group have shown that peptides with the original sequence (LP3, H-^{1127}GDNDSEDNSDEENC^{1134}-$CONH_2$) of the extracelular chain (cluster II, domain CR9) of LRP1, as well as its derived

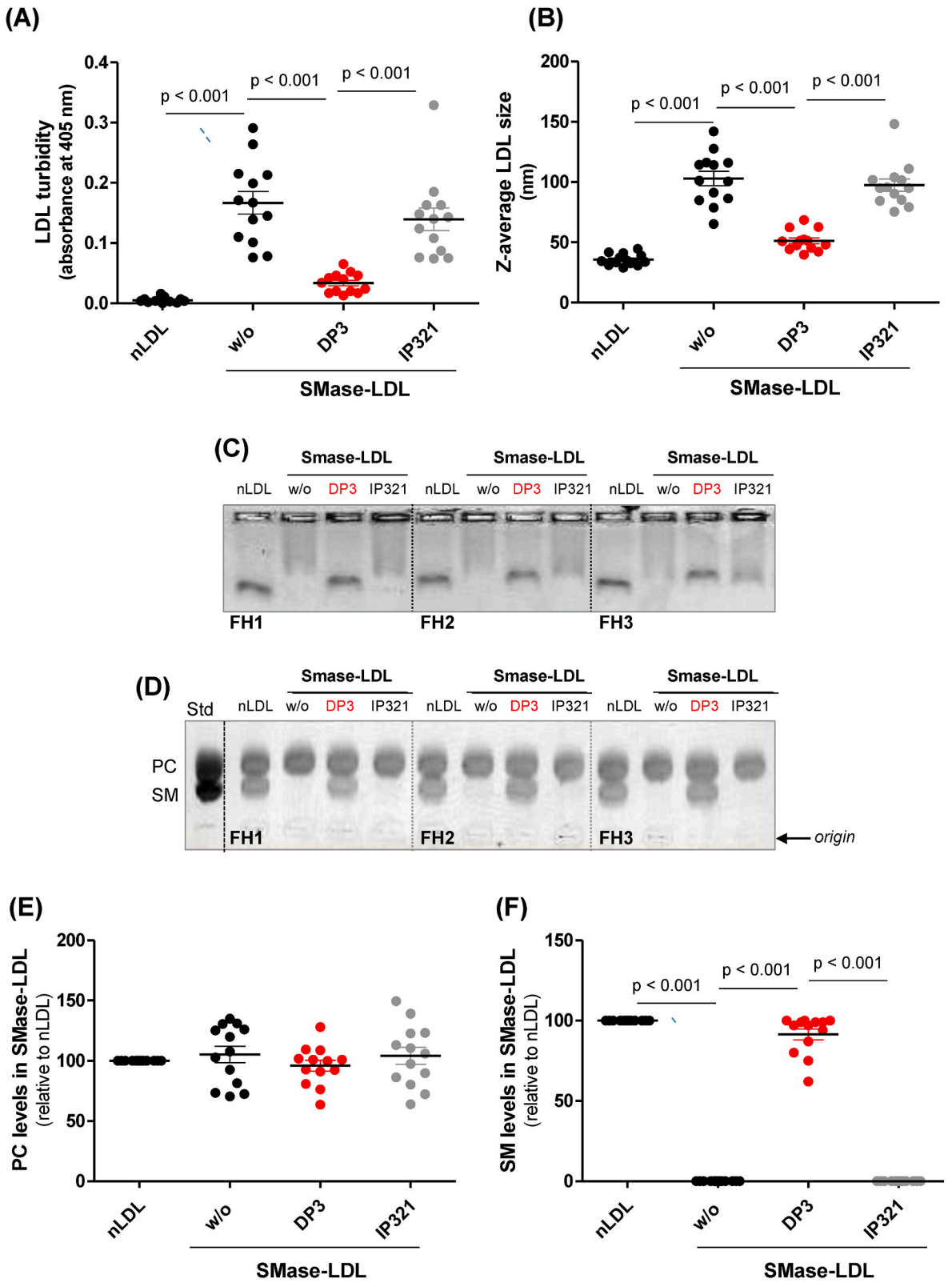

Fig. 6. DP3 reduces SMase-induced aggregation of LDL from patients with familiar hypercholesterolemia (FH).
LDL isolated from each patient was untreated (LDL) or treated with SMase (40 U/L) in the absence or presence of DP3 and IP321 (10 μM, peptide/ApoB100 ratio: 4.7:1). (A) Effects of DP3 on the area under the curve (AUC) of turbidimetry induced by exposure of LDL to SMase for increasing times (24, 48, and 72 h). Data are mean ± SD of LDL isolated from 13 patients. (B) Effects of DP3 on the Z-average LDL size measured in a Zetasizer Nano ZS equipment. (C) Representative agarose gel showing electrophoretic mobility of human LDL (2 μg/well) in agarose gels (0.5 %) that were dehydrated and stained with Coomassie blue. (D) Representative High-performance thin layer chromatography (HPTLC) analysis of LDL phospholipid lipid content and graphs showing the mean ± SD of PC (E) and SM (F) levels. n = 13/group. Differences between groups were analyzed using Student's *t*-test for independent samples. PC: phosphatidylcholine, SM: sphyngomyelin. Std: standards. (For interpretation of the references to color in this figure legend, the reader is referred to the Web version of this article.)

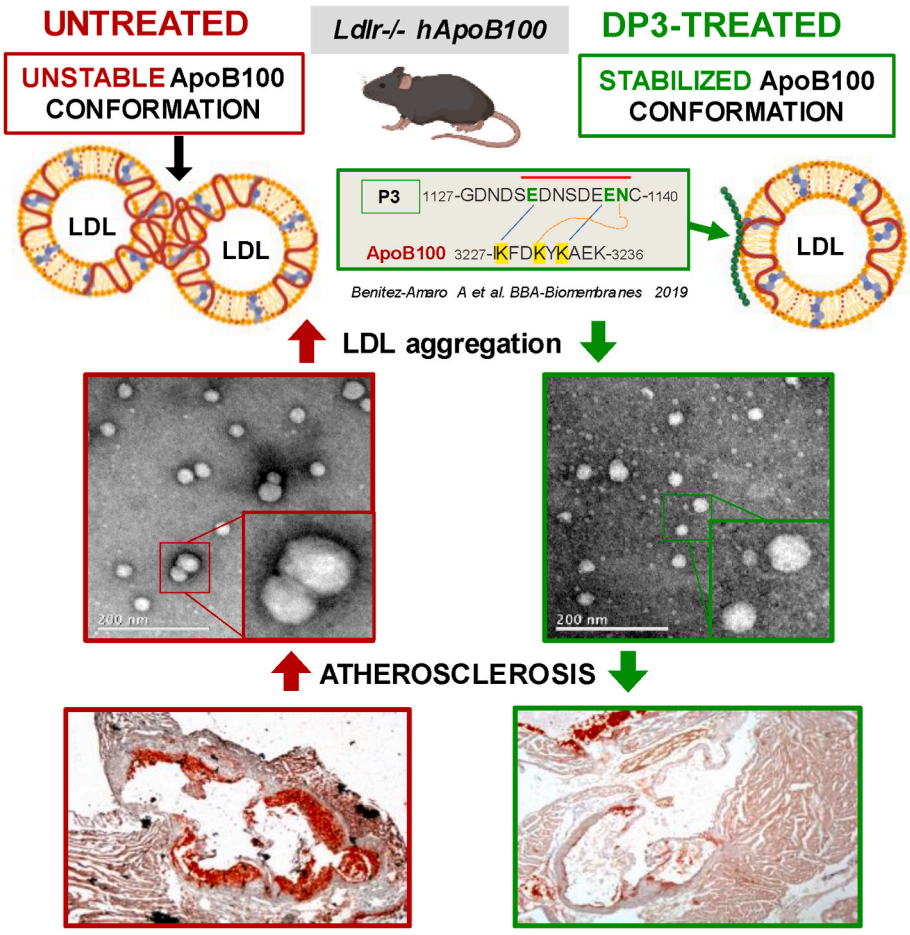

Fig. 7. Summary diagram illustrating the proposed mechanisms by which DP3 exerts its anti-atherosclerotic effects in the *Ldlr*$^{-/-}$*hApoB100* transgenic mouse model. DP3 effectively inhibits atherosclerosis through mechanisms that include stabilization of ApoB100 conformational structure and preservation of LDL integrity.

retro-*enantio* version (DP3, H-needsndesdndh-$CONH_2$), efficiently inhibit LDL aggregation induced by SMase and PLA_2 and foam cell formation from human coronary vascular smooth muscle cell formation [19]. The high anti-LDL aggregation efficacy of these peptides is caused by their capacity to establish electrostatic interactions with the ^{3227}IKFDKYKAEK^{3236} sequence of ApoB100, forming a stable DP3: ApoB100 complex that guarantees the maintenance of ApoB100 conformation in human LDL [18,19]. This specific ApoB epitope (Ile^{3227}-Lys^{3236}) is absent in ApoB48, since this shorter ApoB protein variant is produced after RNA editing of the apoB100 transcript at residue 2180 [41].

Circular Dichroism (CD) analysis conducted in this study showed that DP3 significantly affects the conformation of ApoB100 in LDL from the humanized murine model. ApoB100 in LDL from DP3-injected mice exhibited a higher percentage of α-helix secondary structures, both in unexposed and SMase-exposed LDL, compared to ApoB100 in LDL from control groups. Since amphipathic alpha-helices and beta sheets are major lipid-associating motifs of ApoB100 [42,43], maintaining α-helical domains in ApoB100 appears crucial for preserving LDL integrity. Additionally, Western blot analysis revealed that ApoB100 epitopes in LDL from the DP3 group had significantly lower accessibility to anti-ApoB100 antibodies compared to LDL from control groups. Together, these results suggest that, as previously shown in *in vitro* studies with human LDL [18,19], DP3 efficiently preserves the structural conformation of ApoB100 *in vivo* in the LDL of hapoB100 Tg mice.

Measurements of Z-Potential and electrophoretic mobility of LDL from the three experimental mouse groups indicated that neither DP3 nor IP321 altered the charge of murine LDL particles. Although DP3 is negatively charged, the epitope (Ile3227-Lys3236) to which DP3 binds occurs only once in the entire ApoB100 sequence, suggesting that only one peptide binds per ApoB100 protein. Furthermore, the DP3/ApoB100 complex is primarily stabilized by salt bridge interactions between two acidic residues in DP3 (D-Glu3 and D-Glu9) and two positively charged residues in ApoB100 (Lys3229 and Lys3234) [18]. These interactions likely explain why DP3 binding to ApoB100 does not alter the net charge of LDL particles. Although the Z-Potential of LDL was not altered by peptide treatment, it was significantly changed by exposure to SMase, regardless of the experimental group. The phospholypolysis of sphingomyelin (SM) by sphingomyelinase (SMase) generates ceramide, a more hydrophobic molecule that interacts less effectively with the surrounding aqueous environment of low-density lipoproteins (LDL). This shift in LDL composition may expose polar groups on other regions of the particle, thereby altering its Z-potential. Additionally, the degradation of SM could induce conformational changes in apolipoproteins on the LDL surface, further modifying the particle's charge distribution.

In contrast to human LDL, DP3 did not effectively prevent sphingomyelin (SM) phospholysis induced by SMase in murine LDL. The lower SM content and smaller LDL size in murine LDL compared to human LDL may contribute to this species-specific difference in DP3's protective effect against phospholypolysis. Notably, we previously observed that DP3 did not protect human LDL from phospholysis induced by PLA2, yet it still exerted strong anti-aggregation effects [18]. Similarly, in murine LDL exposed to SMase, DP3 preserved the ApoB100 conformational structure, which appears to protect LDL from aggregation even under conditions of phospholysis, akin to the effects seen in human LDL

exposed to PLA2 [18].

The lack of a DP3-induced change in the net charge of ApoB100 and the presence of a distinct epitope in ApoB100 (Arg^{3385}-Lys^{3393}) that binds to the LDL receptor (LDLR) [44,45], which is separate from the ApoB100 epitope (Ile^{3227}-Lys^{3236}) interacting with DP3 [18], explains why DP3 does not alter LDL uptake by LDLR, as observed in vascular cells. These findings support the ability of DP3 to maintain the conformational integrity of ApoB100 in LDL.

In our experimental conditions, DP3 did not affect the *ex_vivo* interaction of LDL with proteoglycans. Previous studies have identified site B (residues 3359–3369) in ApoB100 as the primary proteoglycan-binding sequence [46], which is distant from the DP3-binding epitope. Since the interaction of LDL with proteoglycans is crucial in the development and progression of atherosclerosis [47,48], combining anti-LDL aggregation peptides like DP3 with inhibitors of LDL/proteoglycan interactions may be necessary to achieve optimal anti-atherosclerotic effects.

In vivo biodistribution experiments revealed that DP3 is eliminated from the body of *Ldlr*$^{-/-}$ *hApoB100* mice mostly through the kidney, like most peptides [49,50]. Here, we also show that DP3 reached the main tissues of the body, although with differential kinetics; specifically, DP3 was detected transiently (at 15-min post-injection) in aorta and brain, and detected over longer periods in heart and liver. Confocal microscopy images of atherosclerotic plaques showed the presence of TAMRA-DP3 in the arterial intima colocalizing with retained hApoB100, suggesting that DP3 interacts with hApoB100 in the arterial intima of this model.

Immunohistochemical data from the current study demonstrate that daily administration of DP3 led to a more than 75 % reduction in atherosclerotic plaque area without affecting the lipid and lipoprotein profiles or hepatic neutral lipid content in this experimental model. Additionally, there were no significant changes in systemic inflammation, as indicated by peripheral monocyte counts, or in hepatic expression of pro-inflammatory genes (CD36, TNFa, CCL-2, and CD68) between DP3-treated and control groups.

Furthermore, our results indicate that DP3 is effective in preventing LDL aggregation *ex vivo* in LDL from patients with familial hypercholesterolemia (FH). While additional preclinical studies are needed to confirm these findings, our results suggest promising potential for developing new treatments that focus on preserving LDL quality, specifically the structural conformation of ApoB100, for improved management of cardiovascular disease in FH patients. As summarized in Fig. 7, our results demonstrate that by maintaining the ApoB100 structural conformation, DP3 peptides efficiently preserve the quality of LDL and reduce HFD-induced atherosclerosis, thereby highlighting the potential use of LRP1-based peptides as anti-atherosclerotic drugs in the context of familiar hypercholesterolemia.

Author contributions

ABA, EG, RP and JCE-G developed the humanized ApoB100 murine model and performed the peptide administration procedure. EG, ABA, MTLC-L, and AM prepared and obtained the results from the molecular, lipidic, immunohistochemical and confocal studies performed in tissue samples. MTLC-L, CB, MT and JCE-G isolated the lipoproteins from the experimental model and from patients, and performed the biochemical and molecular analysis in isolated lipoproteins. EG, PC and MVC performed *in_vivo* and *ex_vivo* IVIS bioimaging studies. AC and FC selected and included the pacients in the study and collected serum samples. AP and BB processed and analyzed CD spectra. ABA, EG, JCE-G, RP and VLl-C designed the research and analyzed the data; VLl-C wrote the paper.

Data availability

The data underlying this article will be shared on reasonable request to corresponding author.

Financial support

The economic support to develop this project was received from FIS PI21/01523 (to VLl-C) and PI20/00623 (to MVC) from the Instituto de Salud Carlos III (ISCIII) and co-financed with ERDFs, and Fundación BBVA Ayudas a equipos de investigación 2019, and grants 2021SGR-Cat 00976 from AGAUR, Generalitat de Catalunya) (to MVC). ABA is a postdoctoral fellow (FI19/00205) that was granted by the Programme _Contratos predoctorales de formación de investigación en salud_from the Instituto de Salud Carlos III (ISCIII) and co-financed with ERDFs. M. V·C. was granted by a Miguel Servet contract (MSII/00007) from the Instituto de Salud Carlos III (ISCIII) and PC (FI21/00146) is a predoctoral fellow supported by the Programme_Contratos predoctorales de formación de investigación en salud_from ISCIII and co-financed with ERDFs. EG and MTLC-L were granted by the Ministry of Science, Innovation and Universities of Spain through the FPU predoctoral grants FPU21/01173 and FPU22/01888, respectively. Our group is part of CIBER Enfermedades Cardiovasculares (CIBERCV; CB16/11/00276 to VLl-C) and CIBER Diabetes y Enfermedades Metabólicas Asociadas (CIBERDEM; CB07/08/0016 to JCE-G), projects run by the Instituto de Salud Carlos III. Our group also participates in Redes de investigación (Enfermedades Metabóloicas y Cáncer RED2018-102799-T), a project run by MINECO. We belong to a group recognized by Generalitat de Catalunya (2021 SGR 00834). IR-SANTPAU is a centre of CERCA Programme/Generalitat de Catalunya.

Declaration of competing interest

All authors have read and approved submission of the manuscript and the manuscript has not been published and is not being considered for publication elsewhere in whole or part in any language except as an abstract. None of the authors have any conflict of interest with the publication of the manuscript.

Acknowledgements

The authors thank the crucial support of Dr. Jose Amable Bernabé Mateos from Instituto de Ciencia de Materiales de Barcelona (ICMAB-CSIC) and U6 Biomaterial Processing and Nanostructuring Unit of CIBER BBN for his help in the development of Dynamic Light Scattering experiments.

Appendix A. Supplementary data

Supplementary data to this article can be found online at https://doi.org/10.1016/j.atherosclerosis.2024.118630.

References

[1] M. Gustafsson, J. Borén, Mechanism of lipoprotein retention by the extracellular matrix, Curr. Opin. Lipidol. 15 (2004) 505–514, https://doi.org/10.1097/00041433-200410000-00003.

[2] K. Tran-Lundmark, P.K. Tran, G. Paulsson-Berne, V. Fridén, R. Soininen, K. Tryggvason, et al., Heparan sulfate in perlecan promotes mouse atherosclerosis: roles in lipid permeability, lipid retention, and smooth muscle cell proliferation, Circ. Res. 103 (2008) 43–52, https://doi.org/10.1161/CIRCRESAHA.108.172833.

[3] M. Umaerus, B. Rosengren, B. Fagerberg, E. Hurt-Camejo, G. Camejo, HDL2 interferes with LDL association with arterial proteoglycans: a possible atheroprotective effect, Atherosclerosis 225 (1) (2012) 115–120, https://doi.org/10.1016/j.atherosclerosis.2012.08.040.

[4] S.L. Schissel, J. Tweedie-Hardman, J.H. Rapp, G. Graham, K.J. Williams, I. Tabas, Rabbit aorta and human atherosclerotic lesions hydrolyze the sphingomyelin of retained low-density lipoprotein. Proposed role for arterial-wall sphingomyelinase in subendothelial retention and aggregation of atherogenic lipoproteins, J. Clin. Invest. 98 (1996) 1455–1464, https://doi.org/10.1172/JCI118934.

[5] M. Sneck, S.D. Nguyen, T. Pihlajamaa, G. Yohannes, M.L. Riekkola, R. Milne, et al., Conformational changes of apoB-100 in SMase-modified LDL mediate formation of large aggregates at acidic pH, J. Lipid Res. 53 (2012) 1832–1839, https://doi.org/10.1194/jlr.M023218.

[6] V. Llorente-Cortés, M. Otero-Viñas, E. Hurt-Camejo, J. Martínez-González, L. Badimon, Human coronary smooth muscle cells internalize versican-modified

LDL through LDL receptor-related protein and LDL receptors, Arterioscler. Thromb. Vasc. Biol. 22 (2002) 387–393, https://doi.org/10.1161/hq0302.105367.
[7] V. Llorente-Cortés, M. Otero-Viñas, S. Sánchez, C. Rodríguez, L. Badimon, Low-density lipoprotein upregulates low-density lipoprotein receptor-related protein expression in vascular smooth muscle cells: possible involvement of sterol regulatory element binding protein-2-dependent mechanism, Circulation 106 (2002) 3104–3110, https://doi.org/10.1161/01.cir.0000041434.28573.0b.
[8] P. Costales, R. Aledo, S. Vérnia, A. Das, V.H. Shah, M. Casado, et al., Selective role of sterol regulatory element binding protein isoforms in aggregated LDL-induced vascular low density lipoprotein receptor-related protein-1 expression, Atherosclerosis 213 (2010) 458–468, https://doi.org/10.1016/j.atherosclerosis.2010.09.034.
[9] J. Castellano, R. Aledo, J. Sendra, P. Costales, O. Juan-Babot, L. Badimon, et al., Hypoxia stimulates low-density lipoprotein receptor-related protein-1 expression through hypoxia-inducible factor-1α in human vascular smooth muscle cells, Arterioscler. Thromb. Vasc. Biol. 31 (2011) 1411–1420, https://doi.org/10.1161/ATVBAHA.111.225490.
[10] V. Llorente-Cortés, M. Otero-Viñas, S. Camino-López, O. Llampayas, L. Badimon, Aggregated low-density lipoprotein uptake induces membrane tissue factor procoagulant activity and microparticle release in human vascular smooth muscle cells, Circulation 110 (2004) 452–459, https://doi.org/10.1161/01.CIR.0000136032.40666.3D.
[11] S. Camino-López, V. Llorente-Cortés, J. Sendra, L. Badimon, Tissue factor induction by aggregated LDL depends on LDL receptor-related protein expression (LRP1) and Rho A translocation in human vascular smooth muscle cells, Cardiovasc. Res. 73 (2007) 208–216, https://doi.org/10.1016/j.cardiores.2006.10.017.
[12] M. Ruuth, S.D. Nguyen, T. Vihervaara, M. Hilvo, T.D. Laajala, P.K. Kondadi, et al., Susceptibility of low-density lipoprotein particles to aggregate depends on particle lipidome, is modifiable, and associates with future cardiovascular deaths, Eur. Heart J. 39 (2018) 2562–2573, https://doi.org/10.1093/eurheartj/ehy319.
[13] S.P. Heffron, M.K. Ruuth, Y. Xia, G. Hernandez, L. Äikäs, C. Rodriguez, et al., Low-density lipoprotein aggregation predicts adverse cardiovascular events in peripheral artery disease, Atherosclerosis 316 (2021) 53–57, https://doi.org/10.1016/j.atherosclerosis.2020.11.016.
[14] F. Ursini, K.J. Davies, M. Maiorino, T. Parasassi, A. Sevanian, Atherosclerosis: another protein misfolding disease? Trends Mol. Med. 8 (2002) 370–374, https://doi.org/10.1016/s1471-4914(02)02382-1.
[15] D. de Gonzalo-Calvo, R. Elosua, A. Vea, I. Subirana, S. Sayols-Baixeras, J. Marrugat, et al., Soluble low-density lipoprotein receptor-related protein 1 as a biomarker of coronary risk: predictive capacity and association with clinical events, Atherosclerosis 287 (2019) 93–99, https://doi.org/10.1016/j.atherosclerosis.2019.06.904.
[16] E. Garcia, P. Camps-Renom, N. Puig, A. Fernández-Leon, A. Aguilera-Simón, A. Benitez-Amaro, et al., Soluble low-density lipoprotein receptor-related protein 1 as a surrogate marker of carotid plaque inflammation assessed by ^{18}F-FDG PET in patients with a recent ischemic stroke, J. Transl. Med. 21 (2023) 131–141, https://doi.org/10.1186/s12967-022-03867-w.
[17] P. Costales, P. Fuentes-Prior, J. Castellano, E. Revuelta-Lopez, M.Á. Corral-Rodríguez, L. Nasarre, et al., Domain CR9 of low density lipoprotein (LDL) receptor-related protein 1 (LRP1) is critical for aggregated LDL-induced foam cell formation from human vascular smooth muscle cells, J. Biol. Chem. 290 (2015) 14852–14865, https://doi.org/10.1074/jbc.M115.638361.
[18] A. Benitez-Amaro, C. Pallara, L. Nasarre, A. Rivas-Urbina, S. Benitez, A. Vea, et al., Molecular basis for the protective effects of low-density lipoprotein receptor-related protein 1 (LRP1)-derived peptides against LDL aggregation, Biochim. Biophys. Acta Biomembr. 1861 (2019) 1302–1316, https://doi.org/10.1016/j.bbamem.2019.05.003.
[19] A. Benitez Amaro, C. Pallara, L. Nasarre, R. Ferreira, D. de Gonzalo Calvo, R. Prades, et al., Development of innovative antiatherosclerotic peptides through the combination of molecular modeling and a dual (Biochemical-Cellular) screening system, Advanced Therapeutics 3 (2020) 2000037–2000047, https://doi.org/10.1002/adtp.202000037.
[20] M.S. Brown, J.L. Goldstein, Biomedicine. Lowering LDL–not only how low, but how long? Science 311 (2006) 1721–1723, https://doi.org/10.1126/science.1125884.
[21] A. Benitez Amaro, A. Solanelles Curco, E. Garcia, J. Julve, J. Rives, S. Benitez, et al., Apolipoprotein and LRP1-based peptides as new therapeutic tools in atherosclerosis, J. Clin. Med. 10 (2021) 3571–3581, https://doi.org/10.3390/jcm10163571.
[22] S.D. Nguyen, M. Javanainen, S. Rissanen, H. Zhao, J. Huusko, A.M. Kivelä, et al., Apolipoprotein A-I mimetic peptide 4F blocks sphingomyelinase-induced LDL aggregation, J. Lipid Res. 56 (2015) 1206–1221, https://doi.org/10.1194/jlr.M059485.
[23] M. Martínez-Bujidos, A. Rull, B. González-Cura, M. Pérez-Cuéllar, L. Montoliu-Gaya, S. Villegas, et al., Clusterin/apolipoprotein J binds to aggregated LDL in human plasma and plays a protective role against LDL aggregation, FASEB J 29 (2015) 1688–1700, https://doi.org/10.1096/fj.14-264036.
[24] A. Rivas-Urbina, A. Rull, L. Montoliu-Gaya, M. Pérez-Cuellar, J. Ordóñez-Llanos, S. Villegas, J.L. Sánchez-Quesada, Low-density lipoprotein aggregation is inhibited by apolipoprotein J-derived mimetic peptide D-[113-122] apoJ, Biochim. Biophys. Acta Mol. Cell Biol. Lipids 1865 (2020) 158541–158548, https://doi.org/10.1016/j.bbalip.2019.158541.
[25] A. Benitez-Amaro, N. Martínez-Bosch, N. Manero-Rupérez, L. Claudi, M.T. La Chica Lhoëst, M. Soler, et al., Peptides against low density lipoprotein (LDL) aggregation inhibit intracellular cholesteryl ester loading and proliferation of pancreatic tumor cells, Cancers 14 (2022) 890–895, https://doi.org/10.3390/cancers14040890.
[26] A.K. Ruotsalainen, J.P. Lappalainen, E. Heiskanen, M. Merentie, V. Sihvola, J. Näpänkangas, et al., Nuclear factor E2-related factor 2 deficiency impairs atherosclerotic lesion development but promotes features of plaque instability in hypercholesterolaemic mice, Cardiovasc. Res. 115 (2019) 243–254, https://doi.org/10.1093/cvr/cvy143.
[27] J.A. Gómez-Gerique, J.A. Gutiérrez-Fuentes, M.T. Montoya, A. Porres, A. Rueda, A. Avellaneda, et al., Perfil lipídico de la población española: estudio DRECE (Dieta y Riesgo de Enfermedad Cardiovascular en España). Grupo de estudio DRECE [Lipid profile of the Spanish population: the DRECE (diet and risk of cardiovascular disease in Spain) study. DRECE study group], Med. Clin. 113 (1999) 730–735.
[28] M. Cuchel, E. Bruckert, H.N. Ginsberg, F.J. Raal, R.D. Santos, R.A. Hegele, et al., European Atherosclerosis Society Consensus Panel on Familial Hypercholesterolaemia, Homozygous familial hypercholesterolaemia: new insights and guidance for clinicians to improve detection and clinical management. A position paper from the Consensus Panel on Familial Hypercholesterolaemia of the European Atherosclerosis Society, Eur. Heart J. 35 (2014) 2146–2157, https://doi.org/10.1093/eurheartj/ehu274.
[29] A. Daugherty, A.R. Tall, M.J.A.P. Daemen, E. Falk, E.A. Fisher, G. García-Cardeña, et al., American Heart Association Council on Arteriosclerosis, Thrombosis and Vascular Biology; and Council on Basic Cardiovascular Sciences, Recommendation on design, execution, and reporting of animal atherosclerosis studies: a scientific statement from the American heart association, Arterioscler. Thromb. Vasc. Biol. 37 (2017) e131–e157, https://doi.org/10.1161/ATV.0000000000000062.
[30] M.R. Hamczyk, R. Villa-Bellosta, P. Gonzalo, M.J. Andrés-Manzano, P. Nogales, J. F. Bentzon, et al., Vascular smooth muscle-specific progerin expression accelerates atherosclerosis and death in a mouse model of hutchinson-gilford progeria syndrome, Circulation 138 (2018) 266–282.
[31] Y. Wei, A.A. Thyparambil, R.A. Latour, Protein helical structure determination using CD spectroscopy for solutions with strong background absorbance from 190 to 230 nm, Biochim. Biophys. Acta Protein Proteonomics 1844 (2014) 2331–2337, https://doi.org/10.1016/j.bbapap.2014.10.001.
[32] G.S. Getz, C.A. Reardon, Animal models of atherosclerosis, Arterioscler. Thromb. Vasc. Biol. 32 (2012) 1104–1115, https://doi.org/10.1161/ATVBAHA.111.237693.
[33] I. Ilyas, P.J. Little, Z. Liu, Y. Xu, D. Kamato, B.C. Berk, et al., Mouse models of atherosclerosis in translational research, Trends Pharmacol. Sci. 43 (2022) 920–939, https://doi.org/10.1016/j.tips.2022.06.009.
[34] M.M. Véniant, V. Pierotti, D. Newland, C.M. Cham, D.A. Sanan, R.L. Walzem, et al., Susceptibility to atherosclerosis in mice expressing exclusively apolipoprotein B48 or apolipoprotein B100, J. Clin. Invest. 100 (1997) 180–188, https://doi.org/10.1172/JCI119511.
[35] C. Flood, M. Gustafsson, P.E. Richardson, S.C. Harvey, J.P. Segrest, J. Borén, Identification of the proteoglycan binding site in apolipoprotein B48, J. Biol. Chem. 277 (2002) 32228–32233, https://doi.org/10.1074/jbc.M204053200.
[36] D.A. Blasiole, R.A. Davis, A.D. Attie, The physiological and molecular regulation of lipoprotein assembly and secretion, Mol. Biosyst. 3 (2007) 608–619, https://doi.org/10.1039/b700706j.
[37] N.O. Davidson, G.S. Shelness, B. Apolipoprotein, mRNA editing, lipoprotein assembly, and presecretory degradation, Annu. Rev. Nutr. 20 (2000) 169–193, https://doi.org/10.1146/annurev.nutr.20.1.169.
[38] W.R. Fisher, L.A. Zech, P.W. Stacpoole, ApoB metabolism in familial hypercholesterolemia. Inconsistencies with the LDL receptor paradigm, Arterioscler. Thromb. 14 (1994) 501–510, https://doi.org/10.1161/01.atv.14.4.501.
[39] L. Powell-Braxton, M. Véniant, R.D. Latvala, K.I. Hirano, W.B. Won, J. Ross, et al., A mouse model of human familial hypercholesterolemia: markedly elevated low density lipoprotein cholesterol levels and severe atherosclerosis on a low-fat chow diet, Nat Med 4 (1998) 934–938, https://doi.org/10.1038/nm0898-934.
[40] D.A. Sanan, D.L. Newland, R. Tao, S. Marcovina, J. Wang, V. Mooser, et al., Low-density lipoprotein receptor-negative mice expressing human apolipoprotein B-100 develop complex atherosclerotic lesions on a chow diet: no accentuation by apolipoprotein(a), Proc Natl Acad Sci U S A 95 (1998) 4544–4549, https://doi.org/10.1073/pnas.95.8.4544.
[41] K. Higuchi, A.V. Hospattankar, S.W. Law, N. Meglin, J. Cortright, H.B. Brewer Jr., Human apolipoprotein B (apoB) mRNA: identification of two distinct apoB mRNAs, an mRNA with the apoB-100 sequence and an apoB mRNA containing a premature in-frame translational stop codon, in both liver and intestine, Proc Natl Acad Sci U S A 85 (1988) 1772–1776, https://doi.org/10.1073/pnas.85.6.1772.
[42] T. Hevonoja, M.O. Pentikäinen, M.T. Hyvönen, P.T. Kovanen, M. Ala-Korpela, Structure of low-density lipoprotein (LDL) particles: basis for understanding molecular changes in modified LDL, Biochim. Biophys. Acta 1488 (2000) 189–210, https://doi.org/10.1016/s1388-1981(00)00123-2.
[43] J.P. Segrest, M.K. Jones, H. De Loof, N. Dashti, Structure of apolipoprotein B-100 in low density lipoproteins, J. Lipid Res. 42 (2001) 1346–1367. PMID: 11518754.
[44] C.Y. Yang, S.H. Chen, S.H. Gianturco, W.A. Bradley, J.T. Sparrow, M. Tanimura, et al., Sequence, structure, receptor-binding domains and internal repeats of human apolipoprotein B-100, Nature 323 (1986) 738–742, https://doi.org/10.1038/323738a0.
[45] A.V. Hospattankar, S.W. Law, K. Lackner, HBJr Brewer, Identification of low-density lipoprotein receptor binding domains of human apolipoprotein B-100: a proposed consensus LDL receptor binding sequence of apoB-100, Biochem. Biophys. Res. Commun. 139 (1986) 1078–1085, https://doi.org/10.1016/s0006291x(86)80287x. PMID: 3767991.
[46] J. Borén, K. Olin, I. Lee, A. Chait, T.N. Wight, T.L. Innerarity, Identification of the principal proteoglycan-binding site in LDL. A single-point mutation in apo-B100

severely affects proteoglycan interaction without affecting LDL receptor binding, J. Clin. Invest. 101 (1998) 2658–2664, https://doi.org/10.1172/JCI2265.

[47] G. Camejo, E. Hurt-Camejo, O. Wiklund, G. Bondjers, Association of apo B lipoproteins with arterial proteoglycans: pathological significance and molecular basis, Atherosclerosis 139 (1998) 205–222, https://doi.org/10.1016/s0021-9150(98)00107-5.

[48] K. Skålén, M. Gustafsson, E.K. Rydberg, L.M. Hultén, O. Wiklund, T.L. Innerarity, J. Borén, Subendothelial retention of atherogenic lipoproteins in earlybatherosclerosis, Nature 417 (2002) 750–754, https://doi.org/10.1038/nature00804.

[49] B. Bumbaca, Z. Li, D.K. Shah, Pharmacokinetics of protein and peptide conjugates, Drug Metab Pharmacokinet 34 (2019) 42–54, https://doi.org/10.1016/j.dmpk.2018.11.001.

[50] B.J. Tombling, Y. Zhang, Y.H. Huang, D.J. Craik, C.K. Wang, The emerging landscape of peptide-based inhibitors of PCSK9, Atherosclerosis 330 (2021) 52–60, https://doi.org/10.1016/j.atherosclerosis.2021.06.903.